Kinetics of NH_3-oxidation, NO-turnover, N_2O-production and electron flow during oxygen depletion in model bacterial and archaeal ammonia oxidisers

Linda Hink[1], Pawel Lycus[2], Cécile Gubry-Rangin[1], Åsa Frostegård[2], Graeme W. Nicol[3], James I. Prosser[1], Lars R. Bakken[2]

[1] School of Biological Sciences, University of Aberdeen, Cruickshank Building, Aberdeen, AB24 3UU, UK

[2] Faculty of Chemistry, Biotechnology and Food Science, Norwegian University of Life Sciences, 1432, Ås, Norway

[3] Laboratoire Ampère, École Centrale de Lyon, Université de Lyon, 69134, Ecully CEDEX, France

Originality-Significance Statement

The authors confirm that all of the work is original. Ammonia oxidizing bacteria (AOB) and archaea (AOA) contribute to the emission of the greenhouse gas N_2O. Our study corroborate current understanding of the metabolic pathways leading to higher N_2O production by AOB than by AOA, but provides candid assessments of their possible contribution to N_2O emissions through high resolution gas kinetics and product stoichiometry measured under physiologically realistic and ecologically relevant conditions; low cell density and gradual depletion of oxygen. The data also shed new light on the physiological role of the denitrification pathway in AOB; indicating that it plays a negligible role in sustaining their respiratory metabolism; accounting for less than 1.2% of the electron flow even under severe oxygen limitation. A more plausible physiological role for denitrification is redox balancing, which would explain the high N_2O production rates at 4 mM TAN than at 1 mM. An important environmental implication is that the N_2O yield of AOB increases with increasing ammonium concentration, and that fertilizer application level controls the N_2O/NO_2^- product ratio of nitrification in agricultural soils.

Summary

Ammonia oxidising bacteria (AOB) are thought to emit more nitrous oxide (N_2O) than ammonia oxidising archaea (AOA), due to their higher N_2O yield under oxic conditions and denitrification in response to oxygen (O_2) limitation. We determined the kinetics of growth and turnover of nitric oxide (NO) and N_2O at low cell densities of *Nitrosomonas europaea* (AOB) and *Nitrosopumilus maritimus* (AOA) during gradual depletion of TAN ($NH_3 + NH_4^+$) and O_2. Half-saturation constants for O_2 and TAN were similar to those determined by others, except for the half-saturation constant for ammonium in *N. maritimus* (0.2 mM), which is orders of magnitudes higher than previously reported. For both strains, cell-specific rates of NO turnover and N_2O production reached maxima near O_2 half-saturation constant concentration (2-10 µM O_2) and decreased to zero in response to complete O_2-depletion. Modelling of the electron flow in *N. europaea* demonstrated low electron flow to denitrification (≤1.2% of the total electron flow), even at sub-micromolar O_2 concentrations. The results corroborate current understanding of the role of NO in the metabolism of AOA and suggest that denitrification is inconsequential for the energy metabolism of AOB, but possibly important as a route for dissipation of electrons at high ammonium concentration.

Introduction

Emissions of nitric oxide (NO) and nitrous oxide (N_2O) from soil and marine environments are mainly driven by heterotrophic denitrification and aerobic ammonia oxidation (e.g. Hu *et al.,* 2015; Santoro *et al*., 2011; Hink *et al*., 2016). The pathways leading to N_2O and NO emissions from ammonia (NH_3) oxidising organisms are only partially understood and differ between ammonia oxidising bacteria (AOB) and archaea (AOA). Both groups oxidise ammonia to hydroxylamine by ammonia monooxygenase (Prosser, 1989; Vajrala *et al.*, 2013), which is further oxidised to nitrite (NO_2^-) by hydroxylamine dehydrogenase (EC 1.7.2.6; formerly known as hydroxylamine oxidoreductase) in AOB (Hooper *et al*., 1978). Hydroxylamine dehydrogenase has not been identified in AOA, where hydroxylamine oxidation is proposed to involve NO as an essential intermediate. NO is thought to support oxidation of hydroxylamine to two molecules of NO_2^-, one of which is reduced to NO, mediated by nitrite reductase (encoded by *nirK*; Kozlowski *et al.*, 2016a). NO has been speculated to be an enzyme-bound intermediate in AOB (Arp and Stein, 2003; Bock and Wagner, 2006). However, the reaction stoichiometry is identical in both groups (Eq. 1).

$$NH_3 + 1.5O_2 \rightarrow NO_2^- + H^+ + H_2O \qquad \text{(Eq. 1)}$$

While both groups possess a nitrite reductase, most AOB also possess a gene encoding a nitric oxide reductase, thus enabling them to sustain respiratory metabolism under oxygen (O_2) limitation, using NO_2^- and NO as alternative electron acceptors, performing so-called nitrifier denitrification (Arp and Stein, 2003; Stein, 2011). Genes encoding a nitrous oxide reductase have not been identified in the genomes of any cultured ammonia oxidiser, which is consistent with physiological observations (*e.g*. Chain *et al.*, 2003; Norton *et al*., 2008; Walker *et al*., 2010; Campbell *et al*., 2011; Tourna *et al*., 2011; Spang *et al*., 2012). Thus, nitrifier denitrification (by AOB) is hypothetically a strong contributor to N_2O emission from soils, for which there is some circumstantial evidence (Wrage *et al.*, 2001, Kool *et al*., 2011; Zhu *et al*., 2013).

59 During unrestricted aerobic growth, AOB emit a relatively low fraction of the oxidised NH_3-N
60 as N_2O-N (N_2O yield: N_2O-N per NO_2^--N generated from NH_3-N oxidised), ranging from ~0.1%
61 in *Nitrosospira* strains (Jiang and Bakken, 1999; Aakra *et al*., 2001) to ~1% in the type strains
62 *Nitrosospira multiformis* ATCC 25196 and *N. europaea* ATCC 19718 (Jiang and Bakken,
63 1999; Anderson *et al*., 1993). Anderson *et al.* (1993) also reported that 2.6% of NH_3-N oxidised
64 is emitted as NO by *N. europaea*. N_2O production under fully oxic conditions may result from
65 nitrosation reactions involving both hydroxylamine and NO_2^- (Zhu-Barker *et al*., 2015) or
66 incomplete oxidation of hydroxylamine by hydroxylamine dehydrogenase resulting in the
67 production of some NO in addition to the main product NO_2^- (Hooper and Terry, 1979; Hooper
68 *et al*., 1997). Nitrifier denitrification by AOB invariably increases in response to O_2 limitation
69 (Goreau *et al*., 1980; Remede and Conrad, 1990; Anderson et al 1993; Dundee and Hopkins,
70 2001; Wrage *et al.*, 2001; Zhu *et al*., 2013; Stieglmeier *et al*., 2014), most likely through
71 activation of denitrification enzymes whose expression is not completely repressed by oxygen
72 (Whittaker *et al.*, 2000; Yu and Chandran, 2010), the rate possibly being controlled by
73 competition for electrons between denitrification enzymes and terminal oxidases (Anderson et
74 al 1993). AOA produce N_2O during unrestricted aerobic growth through so-called 'hybrid
75 formation', which is assumed to result from a chemical nitrosation reaction involving the
76 ammonia oxidation intermediates hydroxylamine and NO (Stieglmeier *et al*., 2014; Kozlowski
77 *et al*., 2016a). N_2O yield appears to be in the lower range of that for AOB; i.e. 0.004 – 0.23%
78 (Jung *et al.,* 2011; Santoro *et al*., 2011; Kim *et al*., 2012; Jung *et al*., 2014; Stieglmeier *et al*.,
79 2014) with no or only marginal increase observed under O_2 limitation (Jung *et al.,* 2011;
80 Löscher *et al*., 2012; Stieglmeier *et al.,* 2014, Qin *et al*., 2017). Both emissions of NO and the
81 capacity to consume external NO have been observed in AOA cultures, consistent with NO
82 being an intermediate during ammonia oxidation (Martens-Habbena *et al*., 2015; Kozlowski *et*
83 *al.*, 2016a).

84 NO turnover and N_2O production are therefore tightly connected to oxidation of NH_3 to NO_2^- in
85 both AOA and AOB, since electrons used during respiration are delivered by the oxidation of

hydroxylamine. As a consequence, AOB cannot sustain nitrifier denitrification under complete anoxia, as confirmed by Anderson *et al*. (1993) for *N. europaea*, but this is apparently contradicted by Kozlowski *et al*. (2016a; 2016b), who invariably observed sharp increases in NO and N_2O production after fast O_2 depletion in micro-respirometry experiments with high cell densities.

To determine the effect of O_2 availability on NO turnover and N_2O production by AOB and AOA over longer time scales and at lower cell densities, a robotised incubation system (Molstad *et al*., 2007) was used. Batch cultures (AOB: *N. europaea*, AOA: *N. maritimus*) with low initial cell concentrations were monitored over periods of 4 - 10 days as they gradually became limited by either O_2 or NH_3. The experiments were designed to determine the affinities for O_2 and ammonium, the product stoichiometry as controlled by the concentration of O_2, and to test specific hypotheses regarding the contrasts between AOA and AOB described above. N_2O yield in AOB was predicted to increase strongly with decreasing O_2 concentration, but not in AOA. Furthermore, it was hypothesised that cell-specific rates of N_2O production by both AOB and AOA decrease to zero in response to complete depletion of O_2 and that AOA are unable to scavenge NO in the absence of O_2. The nitrifier denitrification rate in AOB was hypothesised to be controlled by competition for electrons between terminal oxidases and nitrite and nitic oxide reductases, which was tested by comparing observed and modelled cell-specific electron flow to nitrifier denitrification as a function of O_2 concentration.

Results

Kinetics of ammonia oxidation, oxygen consumption and NO and N_2O production

Concentrations of NO_2^-, O_2, NO, N_2O and N_2 were determined during batch growth of *N. maritimus* and *N. europaea* as either O_2 or total ammonia nitrogen (TAN, $NH_4^+ + NH_3$) was depleted, depending on their initial concentrations (Fig. 1). In vials with 4 mM TAN (*N. europaea* only; Fig. 1A, D, G and J), TAN was in excess for all initial O_2 concentrations, resulting in depletion of O_2 and NO_2^- production in proportion to cumulative O_2 consumption.

In contrast, cultures containing medium with 1 mM TAN depleted either O_2 (vials initially with ~5 and 7 % O_2), TAN (0.5 and 1 % O_2) or both (3 % O_2).

In the vials with 7% O_2, O_2 consumption increased exponentially during the first 3 and 6 days of incubation of *N. europaea* and *N. maritimus*, respectively, until limited by declining concentrations of TAN. O_2 concentrations continued to decline after TAN depletion, but this was due to sampling dilution only (Supporting Information Fig. S4). These data were used to estimate specific growth rate (μ), cell-specific O_2 consumption rate (V_{O2}) and growth yield (Y) during assumed unrestricted, exponential growth (Supporting Information Table S1). V_{O2} values for *N. europaea* were similar at 1 and 4 mM TAN at ~7 fmol O_2 $cell^{-1}$ h^{-1}. Estimated μ and Y for the 1 mM TAN treatment were ~0.04 h^{-1} and ~9.5 x 10^{12} cells mol^{-1} NO_2^-, respectively, but both were ~23% lower for the 4 mM TAN treatment. This suggests some inhibition of *N. europaea* by NH_4^+/NH_3 at the higher TAN concentration. *N. maritimus* specific growth rate was of the same order as that of *N. europaea and* V_{O2} and Y were one order of magnitude lower and higher, respectively (Supporting Information Table S1). The initial cell densities were 0.5*10^6 and 1*10^6 cells mL^{-1} for *N. europaea* and *N. maritimus*, respectively. Final cell densities in the vials with 5 and 7% O_2 were 10^7 mL^{-1} for *N. europaea* (1 mM TAN) and 5.5*10^7 mL^{-1} for *N. maritimus*.

Nitrite and cell density were measured less frequently than gas concentrations, but based on the validated relationship between cumulative O_2 consumption, NO_2^- accumulation and cell density, O_2 measurements were used to estimate both NO_2^- concentration and cell density at each gas sampling point and the rates between each gas sampling. Thus, measured rates (TAN oxidation or gas production/consumption) could be converted to cell-specific rates. The cell-specific O_2 consumption rates were used to estimate apparent maximum rates (V_{max}) and half-saturation concentrations for O_2 (k_{mO2}) and TAN (k_{mTAN}) according to two-substrate kinetics (Table 1 and Fig. 2). Further validation of the double Michaelis-Menten model is shown by regression of model predictions against measurements (Supporting Information Fig. S5). k_{mO2} was similar for *N. europaea* and *N. maritimus* incubated with 1 mM NH_4^+ (2.35 and 2.13

139 µM, respectively). The estimated k_{mO2} for *N. europaea* would be 3.2 µM, if molecular diffusion
140 towards the cell surface was ignored. This was inconsequential for *N. maritimus*. k_{mTAN} was
141 ~0.2 mM for *N. maritimus* and ~3 times higher for *N. europaea* (Table 1). The high V_{max} value
142 estimated for *N. europaea* at 1 mM TAN (16.1 fmol O_2 $cell^{-1}$ h^{-1}) could not be realised in this
143 experiment, since the initial TAN concentration was only ~2 x k_{mTAN}. At 4 mM TAN (~7 x k_{mTAN}),
144 however, O_2 consumption rates close to V_{max} would be expected. Instead, O_2 consumption
145 rates and growth rates were lower at 4 than at 1 mM TAN and V_{max} estimated using the 4 mM
146 TAN data was only 7.3 fmol O_2 $cell^{-1}$ h^{-1} (Supporting Information Fig. S8), presumably due to
147 partial inhibition by NH_4^+/NH_3 at 4 mM TAN as suggested above.

148 *NO turnover*

149 Production of NO by *N. europaea* was detectable from the beginning of the incubation, with
150 higher rates in the treatments with low initial O_2 concentrations (Figs. 1G and H). Accumulation
151 of NO in *N. maritimus* cultures was delayed and not detected before cultures had accumulated
152 ~5 µmol NO_2^- $vial^{-1}$ (~0.1 mM NO_2^-; Figs. 1F and I). Thus, NO production by *N. europaea* was
153 clearly enhanced by O_2 limitation, while this was not the case for *N. maritimus* (Fig. 3). In
154 response to O_2 depletion, *N. europaea* was able to reduce the NO concentration in some
155 treatments (vials with 1 mM TAN and 0.5 and 1 % O_2. Fig 1G and H). In contrast, *N. maritimus*
156 was clearly unable to consume NO once O_2 was depleted. In response to TAN depletion (vials
157 with initial concentrations of 5 and 7% O_2), both strains depleted NO rapidly. *N. europaea*
158 grown at 4 mM TAN produced one order of magnitude more NO than at 1 mM. The contrasting
159 NO kinetics of *N. maritimus* versus *N. europaea* resembles that observed by Kozlowski e*t al*.
160 (2016a) for the contrast between *N. viennensis* (AOA) and *N. multiformis* (AOB); the AOB
161 organism increased its NO production gradually with declining oxygen concentration, while
162 the AOA did not. However, in response to complete oxygen depletion, Kozlowski *et al*. (2016)
163 observed a sharp increase in NO for AOA, while this was clearly not the case for our strain.

The ability to consume NO in response to TAN depletion is better illustrated by cell-specific NO production rates after accounting for sampling dilution and NO autoxidation (Figs. 3A and B). The cell-specific NO production rate was more than one order of magnitude higher in *N. europaea* than in *N. maritimus* and the two strains responded somewhat differently to O_2 and TAN depletion. Production of NO by *N. europaea* increased with decreasing O_2 concentration, reaching a maximum at O_2 concentrations around k_{mO2} (~2 µM). At very low O_2 concentration (<1 µM), there was net consumption (reduction) of NO in *N. europaea*, but this ceased when O_2 concentration approached zero (insert in Fig. 3A). These phenomena were not observed in *N. maritimus*, whose NO production appeared to peak at high cell densities, rather than being dependent on O_2. Both strains were able to reduce NO in response to TAN depletion as also observed for *N. maritimus* by Martens Habenna *et al*. (2015).

N_2O production kinetics and yield

Accumulation of N_2O was detectable immediately after incubation initiation of all cultures and production ceased as ammonia oxidation rate decreased, due to O_2 and/or TAN limitation (Figs. 2J, K and L). N_2O remained in the headspace in all cultures until the end of the incubation, and N_2 production was not detected. The apparent reduction of N_2O after TAN depletion was due to losses from sampling (dilution of the headspace by helium replacing sampled gas). In contrast, N_2O concentration remained almost constant after O_2 depletion. This reflects low but continued N_2O production, probably driven by minor inputs of O_2 at each sampling (~40 nmol per sampling).

The cell-specific rate of N_2O production in both strains increased with decreasing O_2 concentration, reaching maximum values at O_2 concentrations around the apparent k_{mO2}, and rapidly declined towards zero at lower O_2 (Figs. 3C and D). The two strains reacted differently to TAN depletion: while N_2O production by *N. europaea* declined with declining TAN concentration (vials with 3, 5 and 7% O_2), N_2O production by *N. maritimus* appeared unaffected by TAN concentration until this approached k_{mTAN} (~0.2 mM). This contrast between

190 the two strains is better illustrated in Fig. 4, showing the relation between specific N_2O
191 production rate (V_{N2O}) and V_{O2}. In *N. maritimus*, V_{N2O} was almost proportional to V_{O2} for all
192 treatments within the V_{O2} range 0 - 0.6 fmol O_2 cell^{-1} h^{-1}. It should be noted that O_2 consumption
193 rate in the 5 and 7% O_2 treatments became limited by TAN rather than O_2, while the opposite
194 was the case for the 0.5 and 1% O_2 treatments. Thus, N_2O production in *N. maritimus* declined
195 in proportion to the rate of nitrification, independent of the limiting factor (O_2 or TAN). This was
196 not the case for *N. europaea*, where trajectories were widely different for the different O_2
197 treatments, with higher V_{N2O} at lower O_2 tension.

198 N_2O yield (Y_{N2O}) was estimated for each time increment. Y_{N2O} increased as O_2 concentration
199 approached zero for both *N. europaea* and *N. maritimus* (Fig. 5), although the levels were
200 widely different (*N. maritimus* < *N. europaea* 1 mM TAN < *N. europaea* 4 mM TAN). As noted
201 above, Y_{N2O} for *N europaea* fell towards zero as TAN was depleted (3, 5 and 7% O_2 treatments,
202 Fig. 5A), while this was not the case for *N. maritimus* (Fig. 5C).

203 *Electron flow to nitrifier denitrification*

204 NO and N_2O production in *N. europaea* were modelled based on the assumption that they are
205 controlled by the competition for electrons between terminal oxidases and denitrification
206 enzymes, as controlled by O_2 concentration. Since measured N_2O could be derived from both
207 nitrifier denitrification and incomplete oxidation of hydroxylamine, the latter was included in the
208 model along with nitrifier denitrification and the total rate of N_2O and NO production
209 (measured) was converted to electron flow (2 electrons per N_2O-N, 1 electron per NO), to be
210 compared with model predictions. A simplified model was obtained by assuming identical
211 affinity for cytochrome oxidase ($k_{mD} = k_{mTO}$, see Experimental procedures Eqs. 5 and 6); hence
212 the two pathways only compete for electrons by having different V_{max}. Fig. 6 compares electron
213 flow to nitrifier denitrification (V_{eD}) based on measurements and predictions of the fitted model
214 (r^2 = 0.48; Supporting Information Fig. S6). The model captured the declining V_{eD} with declining
215 TAN (treatments with 5 and 7% O_2) and increasing V_{eD} with declining O_2 concentration, but

failed to capture the declining V_{eD} with declining O_2 concentration within the very low range (inserted panel in Fig. 6). Further, the model predicted 2- to 3-fold lower V_{eD} than that measured in the 4 mM TAN experiment (Supporting Information Fig. S10).

The alternative model, assuming that terminal oxidases (TO) and denitrification enzymes (D) have different affinities for cytochrome C_{552}, was tested by simulating steady state concentrations of reduced cytochrome c_{552} (C^*_{552}) (Supporting information Fig. S8). This gave a similar response to that shown, assuming maximum electron flow to denitrification enzymes (V_{maxeD}) and to terminal oxidases (V_{maxeTO}) to be 3 and 20 fmol e^- $cell^{-1}$ h^{-1}, respectively, and $k_{mD} = 70*k_{TO}$, i.e. that TO has a stronger affinity than D (for C^*_{552}) (see Experimental procedures Eqs. 5 and 6). The discrepancy between model and measurement for the O_2 concentration range 0 - 4 µM (inserted panel in Fig. 6) could be eliminated by reducing k_{mO2} to 0.4 µM and increasing V_{maxeD} by a factor of 4, which is effectively assuming expression of high affinity terminal oxidases and more denitrification enzymes in response to low O_2 concentrations.

It is worth noticing that the estimated V_{eD} (as measured) was very low compared to the total electron flow ($V_{eD} + V_{TO}$); the percentage of electrons directed to denitrification was ~0.3% for $[O_2]_s \geq 50$ µM, increasing gradually with declining O_2 concentrations to reach a maximum of ~1.2 % at $[O_2]_s = 4$ µM (Supporting Information Fig S7).

Discussion

Use of a robotised incubation system enabled monitoring of O_2, NO, and N_2O kinetics by frequent sampling of headspace gas of parallel batch cultures of model archaeal and bacterial ammonia oxidisers as they grew and gradually depleted O_2 and/or TAN. This enabled determination of kinetic parameters for O_2 consumption as a function of concentrations of O_2 and TAN, assuming a simple dual-substrate Michaelis-Menten function (see Experimental Procedures Eq. 4). With one exception, the half-saturation constants were in reasonable agreement with values found by others: a k_{mO2} ~2 µM O_2 for *N. maritimus* is comparable with 3.9 µM O_2 determined by Martens-Habbena *et al.* (2009), and in the lower the range of 1 - 15

242 μM O_2 determined for *N. europaea* (Loveless and Painter, 1968) and *N. europaea*-NOB-mixed
243 cultures (Laanbroek and Gerards, 1993; Laanbroek *et al*., 1994). Similarly, k_{mTAN} = 0.57 mM
244 TAN for *N. europaea* is in the lower range of previously determined values (0.55 - 3.56 mM
245 TAN; Laanbroek and Gerards, 1993; Laanbroek *et al*., 1994; Martens-Habbena *et al*., 2009).
246 However, the k_{mTAN} value of 0.21 mM TAN for *N. maritimus* is three orders of magnitude higher
247 than that determined by Martens-Habbena *et al*. (2009). This major difference is not easy to
248 explain. The strain, growth medium and incubation temperature (30 ^oC) were the same and
249 generated near-identical estimated maximum specific growth rates (0.027 versus 0.028 h^{-1}) in
250 batch culture and comparable half-saturation constants for O_2 (2.2 versus 3.9 μM O_2).
251 However, Martens-Habbena *et al.* (2009) estimated k_{mTAN} by measurement of NH_4^+ uptake
252 rates and O_2 consumption rates following addition of NH_4^+ to suspensions of starving cells at
253 high cell density. Their k_{mTAN} values therefore reflected the influence of TAN concentration on
254 specific cell activity rather than on specific growth rate in our study. Their cultures, unlike ours,
255 were not stirred, which may have influenced diffusion of oxygen or ammonia, particularly at
256 high cell densities, and their O_2 concentrations were higher (150 - 170 μM O_2) than in our
257 experiments, in which the cells depleted TAN at O_2 concentrations of ~20 and 40 μM O_2 (in
258 the 5 and 7% initial O_2 treatments, Fig. 3), but this is unlikely to explain the high k_{mTAN} in our
259 experiment. The ability of our strain to grow with agitation at similar maximum specific growth
260 rate to the static cultures of Martens-Habbena *et al.* (2009) suggests some evolution or
261 'domestication' of the strain during repeated subculturing. This raises the possibility that the
262 strain may also have adapted in other ways to continued laboratory since its use in the study
263 by Martens-Habbena *et al.* (2009). The explanation for these contrasting results is crucial,
264 since our data could be taken to challenge the accepted view that all AOA have significantly
265 higher affinity for TAN than AOB.

266 The O_2 consumption rate of *N. europaea* grown at 4 mM NH_4^+ was much lower than that
267 predicted by the V_{max} of 17.6 fmol O_2 $cell^{-1}$ h^{-1} and k_{mTAN} of 0.57 mM TAN determined in the 1
268 mM TAN experiment. In theory, this discrepancy could be due to substrate inhibition of

ammonia monooxygenase or anabolic processes (carbon dioxide fixation, protein synthesis). However, previously estimated inhibition constants (k_i) of ammonia oxidation determined from wastewater sludges were 290 – 1,600 µM free NH_3 (Park and Bae, 2009) were several orders of magnitude higher than our highest concentration of 4 mM TAN (equivalent to ~0.14 µM free NH_3). A more plausible explanation is that the capacity of ammonia monooxygenase exceeds that of the anabolic processes (or hydroxylamine dehydrogenase) at high concentrations of TAN (Supporting Information Fig. S9). If so, the cells would potentially accumulate hydroxylamine at high TAN, albeit within limits imposed by hydroxylamine toxicity. Interestingly, Schmidt *et al.* (2004) reported accumulation of hydroxylamine by *N. europaea* up to steady state concentrations of 0.8 M (cytoplasm + periplasm) when provided with 2 mM NH_4^+, although hydroxylamine appeared to be bound to proteins and could only be detected after SDS extraction. Hydroxylamine kinetics deserve further study given their potential importance as an electron donor when cells are exposed to sudden anoxia (discussed below), as well as for the apparent lag in metabolic activity in response to NH_4^+ additions to starved AOB (Chandran and Smets, 2008). Interestingly, the apparent excess capacity for ammonium oxidation would necessitate down-regulation of the expression of *amo* genes or activity of AMO in response to high ammonium concentration. In addition, the electron shunt from c_{554} to terminal oxidases and/or denitrification enzymes (Fig 7, red arrow) could be a necessary dissipation of electrons (suggested by Stein *et al*., 2013) to stabilise the redox status of the cells during upshifts in ammonium concentration.

Many studies have demonstrated increased N_2O production by *N. europaea* and other AOB in response to O_2 limitation (reviewed by Colliver and Stephenson, 2000; Arp and Stein 2003), recently demonstrated to depend on the presence of genes coding for nitric oxide reductase (Kozlowski *et al*., 2016b). The phenomenon is commonly ascribed to 'nitrifier denitrification', i.e. that an increasing fraction of the electrons is passed to nitrite and nitric oxide reductase as the activity of terminal oxidases become limited by low O_2 concentration (Fig. 7). Nitrifier denitrification is thought to be a significant source of N_2O emission from soils, based on indirect

296 evidence provided by the dual isotope signature (^{15}N, ^{18}O) of N_2O (Kool *et al*., 2011; Zhu *et*
297 *al*., 2013). The dual isotope method probably overestimates nitrifier denitrification, however,
298 since it is based on the erroneous assumption that the nitrite produced by ammonium oxidation
299 can only be denitrified by ammonia oxidizing bacteria, not by heterotrophic denitrifiers (Kool
300 et al, 2011). Our ambition was to shed some light on the denitrification capacity of AOB by
301 stringent monitoring of O_2, NO and N_2O while the cultures were allowed to deplete either O_2
302 or TAN. As expected, V_{NO} and V_{N2O} increased with decreasing O_2 concentration, reaching
303 maximal values at O_2 concentrations around k_{mO2} (Figs. 2A and C, Table 1). As O_2
304 concentration decreased further, V_{N2O} declined towards zero, while V_{NO} reached negative
305 values (net reduction) within the concentration range 0 - 1 µM O_2, but returned to zero as O_2
306 was completely depleted. Net reduction of NO is consistent with NO as an intermediate in
307 nitrifier denitrification, and the absence of NO reduction once O_2 is depleted is consistent with
308 the view that ammonia oxidation is the only source of electrons to drive nitrifier denitrification.
309 V_{N2O} and V_{NO} decreased with depletion of TAN (treatments with initial 3, 5 and 7 vol% O_2 in
310 headspace, Fig. 3A and C). In treatments with initial 3, 5 and 7 vol% O_2, V_{O2} decreases
311 primarily due to TAN depletion, while in the other treatments, the decrease is primarily due to
312 O_2 depletion. The latter treatments sustain considerably higher V_{N2O} at intermediate V_{O2}, but
313 all treatments decrease to zero as V_{O2} approach zero. This is further illustrated Fig. 5, where
314 N_2O yield is reduced in response to depletion of TAN, and increase in response to O_2
315 depletion.

316 To extend this study beyond empirical observations of the kinetics, NO- and N_2O-production
317 were modelled as the sum of two processes: 1) incomplete oxidation of hydroxylamine
318 (resulting in a constant fraction of oxidised ammonium released as NO and N_2O) and 2) NO-
319 and N_2O-production via nitrifier denitrification, which depends on competition for electrons
320 between TO and D (Fig. 7). The simplified model, which assumed that the terminal oxidases
321 (TO) and denitrification enzymes (D) have identical affinities for cytochrome C_{552}, was indeed
322 able to capture some of the variation in V_{eD} in the different treatments (Fig. 6) and the

parameters illustrate the overwhelming competitive strength of terminal oxidases compared to denitrification: V_{maxeTO} = 640*V_{maxeD}. Arguably, the reason for the preferential V_{eTO} (versus V_{eD}) could also be different affinities for cytochrome C_{552} (TO stronger than D). Exploration of this with a more elaborate model, which assumed different affinities of TO and D for C_{552} and assumption of V_{maxeTO} = 6*V_{maxeD}, and k_{mD} = 70*k_{TO}, gave a reasonable fit (Supporting Information Fig S8).

The two modelling approaches are gross simplifications of the control of electron flow, but further elaborations of branched electron flow regulation (see Otten *et al*., 1999) were considered meaningless in the absence of direct observations to support such efforts. Nevertheless, modelling provided hypothetical explanations for the marginal denitrification capacity of *N. europaea*: it could either be due to a much lower pool of D than TO, or that the two enzyme systems have widely different affinities for cytochrome oxidases (k_{mTO}<<k_{mD}). Regardless of the mechanism, the empirical data strongly suggest that a marginal fraction of the electron flow is directed to D in *N. europaea*, which underscores speculation by Arp and Stein (2003) that the primary role of the denitrification enzymes is not to sustain respiratory metabolism in response to O_2 depletion.

An interesting aspect of the modelling is the discrepancy for O_2 concentrations <4 µM: while the model predicted increasing V_{eD} with decreasing O_2 concentrations, the data showed the opposite trend (inserted panel Fig. 6.). The discrepancy could reflect a regulatory response to O_2 depletion. Plausible responses to O_2 depletion would be expression of high affinity TO and increased expression of denitrification enzymes, as observed by Beyer *et al*. (2009). To explore this, the model response to lowering the k_{TO} and increasing V_{maxeD} (See Experimental procedures Eqs. 5 and 6) was tested. This showed that the observed increasing V_{eD} with increasing O_2 concentration (in the range 0 - 4 µM) could be obtained by combining an increase in V_{maxeD} by a factor of 4 and a reduction of k_{mO2} from 6 to 0.4 µM O_2 (Supporting information Fig. S7). We acknowledge that the known genetic repertoire for TO in *N. europaea* is limited (Chain *et al*., 2003), possibly lacking genes for high affinity TO.

As mentioned earlier, the electron shunt from HAO to terminal oxidases and/or D (Fig. 7) could be a mechanism of importance for redox balancing at high ammonium concentration, since the cells' capacity to oxidise ammonium at high concentrations apparently exceeds their catabolic capacity. Interestingly, this could explain the high N_2O yield at 4 mM (Fig. 3). A failure of our model to capture this phenomenon could be the gross simplifications made, for instance by assuming a single pool of cytochrome C_{552}.

Our results demonstrate that *N. europaea* has a rather modest capacity to denitrify and rates decrease to zero as O_2 is depleted, as hypothesised. This is somewhat different from the results of Kozlowski *et al*. (2016a; 2016b), who observed substantial N_2O production after complete depletion of O_2. However, their experimental approach was very different, involving concentrated cell suspensions (~10^9 cells mL^{-1}) enclosed in micro-respirometry chambers without headspace, leading to depletion of O_2 from 250 to 0 µM within 5 - 15 minutes. In cultures provided with NH_4^+, they observed high N_2O production rates as O_2 reached undetectable levels (net NO accumulation was marginal compared to N_2O), but the rates decreased gradually throughout the anoxic phase of the experiments, which lasted only 20 - 30 minutes. Their observed initial N_2O production rate for *N. europaea,* immediately after O_2 depletion, was ~0.5 µM min^{-1}, which is equivalent to 30 amol N_2O $cell^{-1}$ h^{-1} (assuming 10^9 cells mL^{-1}, as reported). In terms of electron flow to denitrification (assuming that all N_2O is produced by denitrification), this is equivalent to an electron flow rate of 120 amol $cell^{-1}$ h^{-1}, which is remarkably similar to the maximum rates observed at low O_2 concentrations in our experiments (90 - 95 amol $cell^{-1}$ h^{-1}; Fig. 6). N_2O production rates in two other AOB (*Nitrosomonas sp is79A3* and *Nitrosomonas urea*) were initially 10 - 15 times higher, but were only sustained for minutes, decreasing gradually to ~0.5 µM min^{-1} within 5 - 10 minutes (equivalent to the initial rates for *N. europaea*). Our tentative interpretation of these micro-respirometry results is that observed N_2O production during apparent anoxia could be driven by depletion of hydroxylamine (or other sources of electrons). For a cell to sustain an anoxic electron flow rate of 100 amol h^{-1} for one hour, it would have to contain a minimum of 25 amol

hydroxylamine at the time of O_2 depletion (4 mol electrons available per mol hydroxylamine), which is equivalent to an average concentration of 25 mM in the cytoplasm + periplasm (cell volume ~1 μm^3). In comparison, Schmidt *et al*. (2004) claim that the steady state concentration of hydroxylamine in *N. europaea* when growing aerobically at 2 mM NH_4^+ is around 800 mM (of which 5% was soluble). Thus, fast depletion of O_2, as experienced in short term micro-respirometry experiments, is unlikely to deplete the intracellular hydroxylamine pool, hence nitrifier denitrification under anoxic conditions observed by Kozlowski *et al.* (2016a, 2016b) was plausibly sustained by a gradual oxidation of hydroxylamine (or other alternative sources of electrons). In our experiment, O_2 depletion took hours rather than minutes (Fig. 1), which is likely to have resulted in gradual depletion of hydroxylamine (or any other alternative source of electrons) long before O_2 depletion, explaining the apparent conflict between the two studies.

Modelling of electron flow in *N. maritimus* would hardly be appropriate, since the organism is equipped with nitrite reductase, but not nitric oxide reductase, and the NO produced by nitrite reductase is hypothesised to be consumed as a co-substrate in the oxidation of hydroxylamine to NO_2^- (Kozlowski *et al*., 2016a). The observed kinetics of NO versus nitrification rates allowed inspection of this hypothesis, which would predict a positive feedback on cell-specific nitrification rate via NO accumulation, provided that NO is a free “intermediate”. The results provide little support for such a positive feedback, however (Figs. 1,2,3), which could indicate close interaction between nitrite reductase and Cu-“P460” (the hydroxylamine oxidizing enzyme), i.e. that NO is transferred directly between the two enzymes. Another conspicuous observation is that *N. maritimus* was able to deplete NO in response to the gradual depletion of TAN, but not when depleting oxygen (Fig 1, Fig 3B). This does not necessarily conflict with the model by Kozlowski *et al*. (2016a), but suggests that their model is incomplete regarding NO turnover in these organisms.

Concluding remarks

Our study corroborate current understanding of the metabolic pathways leading to higher N_2O production by AOB than by AOA. The novelty lies in the provision of a candid assessments of their possible contribution to N_2O emissions through high resolution gas kinetics and product stoichiometry measured under physiologically realistic and ecologically relevant conditions; low cell density and gradual depletion of oxygen. The data also shed new light on the physiological role of the denitrification pathway in AOB; indicating that it plays a negligible role in sustaining their respiratory metabolism; accounting for less than 1.2% of the electron flow even under severe oxygen limitation. A more plausible physiological role for denitrification is redox balancing, which would explain the high N_2O production rates at 4 mM TAN than at 1 mM. An important environmental implication is that the N_2O yield of AOB increases with increasing ammonium concentration, and that fertilizer application level controls the N_2O/NO_2^- product ratio of nitrification in agricultural soils.

.

Experimental procedures

Culture strains and medium preparation

The AOB *Nitrosomonas europaea* ATCC 19718 was cultivated in mineral salts medium (Skinner and Walker, 1961) containing 1 mM or 4 mM $(NH_4)_2SO_4$ (equivalent to 50 and 200 µmol TAN $vial^{-1}$, respectively), phenol red (0.5 mg l^{-1}) as an indicator of pH and in addition 10 mM HEPES buffer (10 mM HEPES, 0.6 mM NaOH). pH was initially adjusted to 7.7 - 7.9 by the addition of filter-sterilised Na_2CO_3 that was also added regularly during the batch incubation to adjust the pH. The AOA *Nitrosopumilus maritimus* SCM1 was cultivated in SCM medium (Könneke *et al.*, 2005) supplemented with 1 mM NH_4Cl and buffered at pH 7.5 – 7.6 with 10 mM HEPES buffer. Both media were filter-sterilised and 50 ml medium was placed in

sterile 120-ml serum bottles, each containing a magnetic stirrer flea and sealed with Teflon-coated butyl rubber septa and aluminium caps. The headspace was replaced by helium and the desired volume of pure O_2 was added aseptically as described in Molstad *et al.* (2007). Some carbonate (in equilibrium with carbon dioxide) may have been removed by gas exchange in the headspace but approximately 1 mmol and 0.5 mmol HCO_3^- $vial^{-1}$ remained in *N. europaea* and *N. maritimus* cultures, respectively. These were calculated from the initial carbon dioxide concentration in the headspace, which was 12 – 1,300 ppmv (the concentrations increased throughout incubation in proportion to the oxidation of ammonia associated with proton production leading to slight decline in pH and also ascribed to the regular addition of Na_2CO_3 (*N. europaea* only), results not shown).

Batch incubation, sampling and analysis of gas and liquid samples

Cultures with initial O_2 concentrations of 7%, 5%, 3%, 1%, 0.5% or <0.05% O_2 were prepared with 3 - 5 replicates and were inoculated with 1% (*N. europaea*) or 2% (*N. maritimus*) volumes of mid-exponential phase cultures (initial cell densities were ~0.5 x 10^6 cells ml^{-1} for *N. europaea* and ~10^6 cells mL^{-1} for *N. maritimus*). Triplicate sterile controls with an initial O_2 concentration of <0.05% were included for each experiment. Cultures were incubated in the dark at 30°C while stirring at 200 rpm to provide sufficient gas exchange between headspace and liquid. The incubations were performed in a robotised incubation system that monitors gas concentrations by taking gas samples from the headspace (Molstad *et al.,* 2007; Hassan *et al*., 2016). In short, this was achieved by piercing the septum and pumping the gas through three sampling loops for injection to 1) a chemiluminescence detector for NO, 2) a MolSieve column for separation of N_2 and O_2 (detected by a thermal conductivity detector) and 3) a Plot column for separation of N_2O (detected both by electron-capture and thermal conductivity detectors). After sampling, the pump was reversed and the volume of gas sampled replaced with helium leading to a dilution of the headspace and a marginal leakage of O_2 and N_2 into the system, which is accounted for when calculating gas kinetics. The exact dilution and N_2 and O_2 leakage were determined by including vials filled with high concentrations of N_2 and

455 O_2 (to determine dilution) and with pure He (to determine leakage of N_2 and O_2). These data
456 were taken into account when calculating the rates of gas transport between headspace and
457 liquid.

458 Small liquid samples (~100 µl) were taken under sterile conditions at intervals throughout the
459 incubations for quantification of NO_2^- that was reduced to NO prior to the measurement in a
460 chemiluminescence NO analyser (Roco *et al*., 2016). Samples (~1 ml) were also taken for
461 total cell enumeration by epifluorescence microscopy of DAPI stained cells when cultures were
462 in mid-exponential phase as described in Lehtovirta-Morley *et al*. (2016a).

463 *Gas kinetics calculations*

464 As outlined in detail by Molstad *et al*. (2007), the gas concentration in the liquid during each
465 time interval between two samplings was calculated based on the solubility of each gas (at
466 the given temperature) and the measured transport rate (V; mol s^{-1}), solving Eq. 2 for gas
467 concentration in the liquid ($[G]_l$; mol l^{-1}):

468 $$\boldsymbol{V = k_T \cdot \left(k_H \cdot P_g - [G]_l\right)} \qquad (2)$$

469 where k_T is the transport coefficient (l s^{-1}), k_H is the solubility of the gas (mol l^{-1} atm^{-1}) at the
470 given temperature and P_g is the partial pressure of the gas in the headspace (average for the
471 time increment). The transport coefficient depends on the stirring speed and, for the conditions
472 used (30ºC and 200 rpm stirring), was experimentally determined to be 0.1 l s^{-1} (see Molstad
473 *et al*., 2007). The calculation of gas concentrations in the liquid by Eq. 2 proved essential for
474 O_2, where it was found that $[O_2]_l$ was only 30 - 60% of the equilibrium concentration (k_H*P_g) as
475 the cultures depleted O_2. For NO, $[NO]_l$ reached 120 - 140% of k_H*P_{NO} for the time intervals
476 with rapidly increasing concentrations, but this was essentially inconsequential for the
477 estimated NO per vial, since the solubility of NO is very low (0.0018 mol l^{-1} atm^{-1} at 30ºC). For
478 N_2O, $[N_2O]_l$ reached ~108% of k_H*P_{N2O} for time intervals with rapidly increasing N_2O
479 concentrations (*N. europaea*). Thus, the calculation of liquid concentrations based on

transport was essentially inconsequential for NO and N_2O, but not for O_2, which is important for determination of the affinity for O_2.

The possible consequence of transport limitation for O_2 at the cellular level was assessed, i.e. the molecular diffusion of O_2 from the bulk liquid to the cell surface. This was required because, at high rates of O_2 consumption, it cannot be taken for granted that the concentration at the cell surface is the same as that in the bulk liquid (Hassan *et al*., 2016). Eq. 3 describes the concentration of O_2 at the cell surface ($[O_2]_S$; mol cm^{-3}) of a spherical body (simplification of the rod shaped cells) with radius *r* (cm; $r_{N.\ europaea}$ = 6.4*10^{-5} cm; $r_{N.\ maritimus}$ = 1.7*10^{-5} cm), as a function of $[O_2]_l$ (mol cm^{-3}), the flux towards the cell surface (*J*; mol s^{-1}) and the diffusion coefficient for O_2 in water (*D*; 2.2 *10^{-5} cm^2 s^{-1}).

$$[\boldsymbol{O_2}]_s = [\boldsymbol{O_2}]_l - \frac{\mathbf{1}}{\mathbf{4\pi r D}} \qquad (3)$$

The calculation was essentially inconsequential for *N. maritimus*, since $[O_2]_s$ remained >99% of $[O_2]_l$, but for *N. europaea*, which had higher rates of O_2 consumption, $[O_2]_s$ declined towards ~95 % of $[O_2]_l$ as O_2 concentration approached zero (Supporting Information Fig. S1).

Interpolations

Since cell density and NO_2^- were measured with lower frequency than headspace gas concentration, interpolation was required to calculate NO_2^- concentration and cell density for each time interval between gas samplings. Oxidised TAN and generated NO_2^- were determined using the cumulative O_2 consumption for individual vials. Expected O_2-consumption:NO_2^--production stoichiometry is 1.5:1 (see Eq. 1), which was confirmed by measurements (Supporting Information Fig. S2). Thus, NO_2^- concentration for each time increment between gas samplings was estimated based on cumulated O_2 consumption. The concentration of TAN was estimated by mass balance: $TAN_t = TAN_i - N_{oxt}$, where TAN_t is the amount of TAN per vial at time t, TAN_i is the initial amount and N_{oxt} is N recovered as NO_2^- + NO + N_2O at time t. The measured increase in cell density was a linear function of NO_2^-

505 (Supporting Information Fig. S3). Hence, for each time increment between two gas
506 measurements, measured cumulative O_2 consumption was used to estimate cell density, NO_2^-
507 and TAN concentration. These interpolations enabled modelling of electron flow towards the
508 enzymatically produced N_2O in *N. europaea* (see below).

509 *NO kinetics and autoxidation*

510 NO is unstable under oxic conditions due to autoxidation, which is a "third order" reaction
511 between O_2 and NO, proportional to O_2 concentration and the square of NO concentration
512 (Nadeem *et al*., 2013). As a result, apparent NO production rate (measured as an increase in
513 concentration) may underestimate NO production and apparent NO scavenging (measured
514 as declining NO concentration) may be falsely taken as an indication of NO scavenging by the
515 organisms. To correct for this, NO autoxidation rate was calculated for each time increment,
516 based on Nadeem *et al*. (2013), where NO autoxidation was measured under identical
517 experimental condition to obtain estimates of true enzymatic net production or consumption of
518 NO.

519 *Kinetics*

520 Kinetic constants for whole cell O_2 consumption were estimated on the basis of the measured
521 rates of O_2 consumption, cell abundance and the concentrations of TAN and $[O_2]_s$ for each
522 time interval. Assuming that ammonia monooxygenase is the rate limiting step, two-substrate
523 kinetics is expected, which can be described as a double Michaelis-Menten function
524 (Splittgerber, 1983):

525 $$V_{O_2} = V_{max} \bullet \frac{[O_2]_s}{[O_2]_s + k_{mO2}} \bullet \frac{[TAN]}{[TAN] + k_{mTAN}} \qquad \text{(Eq. 4)}$$

526 where V_{O2} is the rate (fmol O_2 cell^{-1} h^{-1}), V_{max} is the maximum rate (fmol O_2 cell^{-1} h^{-1}), k_{mO2} is
527 the half-saturation constant for O_2 (µM O_2) and k_{mTAN} is the half-saturation constant for TAN

(μM TAN). The parameters were estimated by non-linear regression, using the Levenberger Marquart algorithm in Minitab (Minitab Ltd, UK).

N_2O and NO production by *N. europaea* have been hypothesised to be controlled by O_2 via competition for electrons between terminal oxidases and constitutively expressed denitrification enzymes (Anderson *et al*., 1993). This was investigated by a relatively simple modelling approach (for details see Supporting Information, "Modelling electron flow in *N. europaea* grown at 1 mM TAN" and "Modelling electron flow in *N. europaea* grown at 4 mM TAN"). The branch point was assumed to be the C_{552}, which passes electrons either to denitrification or terminal oxidases (Fig. 7). The model assumes that the flow of electrons to C_{552} (via ubiquinol and *bc1*) is determined by the rate of ammonia oxidation (which is a function of O_2 and TAN concentration) and that the electron flow to the terminal oxidases (TO) and denitrification enzymes (D) is a function of the concentrations of their respective terminal electron acceptors and the concentration of reduced C_{552} ($[C^*_{552}]$), according to Eqs. 5 and 6.

$$\boldsymbol{V_{eD} = V_{maxeD} * \frac{[C^*_{552}]}{[C^*_{552}]+k_{mD}} \bullet \frac{[NO_2^-]}{[NO_2^-]+k_{mNO2}}} \qquad \text{(Eq. 5)}$$

$$\boldsymbol{V_{eTO} = V_{maxeTO} * \frac{[C^*_{552}]}{[C^*_{552}]+k_{mTO}} \bullet \frac{[O_2]}{[O_2]+k_{mO2}}} \qquad \text{(Eq. 6)}$$

where V_{eD} and V_{eTO} are the rates of electron flow to denitrification enzymes and terminal oxidases, respectively, V_{maxeD} and V_{maxeTO} are their maximum rates and their affinity for C^*_{552} is given by their half-saturation constants, k_{mD} and k_{mTO}. Numerical simulation of the steady state concentration of $[C^*_{552}]$ is required unless one assumes that $k_{mNO2} = k_{mO2}$.

Acknowledgments

The authors are members of the Nitrous Oxide Research Alliance (NORA), a Marie Skłodowska-Curie ITN and research project under the EU's seventh framework program

552 (FP7). GN is funded by the AXA Research Fund and CGR by a Royal Society fellowship. We
553 thank Lars Molstad and Peter Dörsch for their generous and invaluable technical assistance.
554 We thank Martin G Klotz for a very constructive review of our paper, and especially for
555 pointing out the possible electron dissipation via periplasmic cytochromes, thus providing a
556 possible explanation for the high N_2O at high ammonium concentrations.
557

558 **Conflict of interests:**

559 None declared
560

561 **References**

562 Aakra, Å., Utåker, J.B. and Nes, I.F. (2001) Comparative phylogeny of the ammonia
563 monooxygenase subunit A and 16S rRNA genes of ammonia-oxidizing bacteria. FEMS
564 Microbiol. Lett. 205:237-242.

565 Anderson, I.C., Poth, M., Homstead, J. and Burdige, D. (1993) A comparison of NO and N_2O
566 production by the autotrophic nitrifier *Nitrosomonas europaea* and the heterotrophic nitrifier
567 *Alcaligenes faecalis*. Appl. Environ. Microbiol. 59:3525-3533.

568 Arp, D. J. and Stein, L.Y. (2003) Metabolism of inorganic N compounds by ammonia-oxidizing
569 bacteria. Criti. Rev. Biochem. Mol. Biol. 38:471-495.

570 Beyer, S., Gilch, S., Meyer, O. and Schmidt, I. (2008) Transcription of genes coding for
571 metabolic key functions in *Nitrosomonas europaea* during aerobic and anaerobic growth. J.
572 Mol. Microbiol. Biotechnol. 16:187-197.

573 Bock, E. and Wagner, M. (2006) Oxidation of inorganic nitrogen compounds as an energy
574 source. In The Prokaryotes. Dworkin, M., Falkow, S., Rosenberg, E., Schleifer, K.-H. and
575 Stackebrandt, E. (eds.). New York: Springer, pp. 457-495.

576 Campbell, M.A., Chain, P.S., Dang, H., El Sheikh, A.F., Norton, J.M., Ward, N. L. *et al*. (2011)
577 *Nitrosococcus watsonii* sp. nov., a new species of marine obligate ammonia-oxidizing bacteria
578 that is not omnipresent in the world's oceans: calls to validate the names 'Nitrosococcus
579 halophilus' and 'Nitrosomonas mobilis'. FEMS Microbiol. Ecol. 76:39-48.

580 Caranto, J.D., Vilbert, A.C. and Lancaster, K.M. (2016) *Nitrosomonas europaea* cytochrome
581 P460 is a direct link between nitrification and nitrous oxide emission. PNAS 113:14704-14709.

582 Chain, P., Lamerdin, J., Larimer, F., Regala, W., Lao, V., Land, M. *et al.* (2003) Complete
583 genome sequence of the ammonia-oxidising bacterium and obligate chemolithoautotroph
584 *Nitrosomonas europaea*. J. Bacteriol. 185:2759-2773.

585 Chandran, K. and Smets, B. F. (2008) Biokinetic characterization of the acceleration phase in
586 autotrophic ammonia oxidation. Water Environ. Res. 80:732-739.

587 Colliver, B.B. and Stephenson, T. (2000) Production of nitrogen oxide and dinitrogen oxide by
588 autotrophic nitrifiers. Biotechnol. Adv. 18:219-232.

589 Dundee, L. and Hopkins, D.W. (2001) Different sensitivities to oxygen of nitrous oxide
590 production by *Nitrosomonas europaea* and *Nitrosolobus multiformis*. Soil Biol. Biochem.
591 33:1563-1565.

592 Goreau, T.J., Kaplan, W.A., Wofsy, S.C., McElroy, M.B., Valois, F.W. and Watson, S.W.
593 (1980) Production of NO_2^- and N_2O by nitrifying bacteria at reduced concentrations of oxygen.
594 Appl. Environ. Microbiol., 40:526-532.

595 Hassan, J., Qu, Z., Bergaust, L. L. and Bakken, L. R. (2016) Transient accumulation of during
596 denitrification explained by assuming cell diversification by stochastic NO_2^- and N_2O
597 transcription of denitrification genes. PLoS Comp. Biol. 12:e1004621.

598 Hink, L., Nicol, G.W. and Prosser, J.I. (2016) Archaea produce lower yields of N_2O than
599 bacteria during aerobic ammonia oxidation in soil. Environ. Microbiol. (in press).

600 Hooper, A.B., Maxwell, P.C. and Terry, K.R. (1978) Hydroxylamine oxidoreductase from
601 *Nitrosomonas*: absorption spectra and content of heme and metal. Biochem. 17:2984-2989.

602 Hooper, A.B. and Terry, K.R. (1979) Hydroxylamine oxidoreductase of *Nitrosomonas*:
603 Production of nitric oxide from hydroxylamine. Biochim. Biophys. Acta Enzymol. 571:12-20.

604 Hooper, A.B., Vanelli, T., Bergmann, D.J. and Arciero, D.M. (1997) Enzymology of the
605 oxidation of ammonia to nitrite by bacteria. Anton. Leeuwenhoek 71:59-67.

606 Hu, H.W., Chen, D. and He, J.Z. (2015) Microbial regulation of terrestrial nitrous oxide
607 formation: understanding the biological pathways for prediction of emission rates. FEMS
608 Microbiol. Rev. 39:729-749.

609 Jiang, Q.Q. and Bakken, L.R. (1999) Nitrous oxide production and methane oxidation by
610 different ammonia-oxidizing bacteria. Appl. Environ. Microbiol. 65:2679-2684.

611 Jung, M.Y., Park, S.J., Min, D., Kim, J.S., Rijpstra, W. I.C., Damsté, J.S.S. *et al.* (2011)
612 Enrichment and characterization of an autotrophic ammonia-oxidizing archaeon of mesophilic
613 crenarchaeal group I. 1a from an agricultural soil. Appl. Environ. Microbiol. 77:8635-8647.

614 Jung, M.Y., Well, R., Min, D., Giesemann, A., Park, S.J., Kim, J.G. *et al.* (2014) Isotopic
615 signatures of N2O produced by ammonia-oxidizing archaea from soils. ISME J. 8:1115-1125.

616 Kim, J.G., Jung, M.Y., Park, S.J., Rijpstra, W.I.C., Sinninghe Damsté, J.S., Madsen, E.L., *et*
617 *al.* (2012) Cultivation of a highly enriched ammonia-oxidizing archaeon of thaumarchaeotal
618 group I. 1b from an agricultural soil. Environ. Microbiol. 14:1528-1543.

619 Klotz, M.G. and Stein L.Y. (2008) Nitrifier genomics and evolution of the nitrogen cycle. FEMS
620 Microbiol. Lett. 278:146-156.

621 Klotz, M.G. and Stein, L.Y. (2010) Genomics of ammonia-oxidizing bacteria and insights into
622 their evolution. In Nitrification. Ward BB, Arp D and Klotz MG (eds). ASM Press, pp 57-93.
623 Könneke, M., Bernhard, A.E., José, R., Walker, C.B., Waterbury, J.B. and Stahl, D.A. (2005)
624 Isolation of an autotrophic ammonia-oxidizing marine archaeon. Nature 437:543-546.

625 Kool D.M., van Groenigen, J.W. and Wrage, N. (2011) Source determination of nitrous oxide
626 based on nitrogen and oxygen isotope tracing: dealing with oxygen exchange. Meth. Enzymol.
627 496:139-160.

628 Kozlowski, J.A., Stieglmeier, M., Schleper, C., Klotz, M.G. and Stein, L.Y. (2016a) Pathways
629 and key intermediates required for obligate aerobic ammonia-dependent chemolithotrophy in
630 bacteria and Thaumarchaeota. ISME J. 10:1836-1845.

631 Kozlowski, J.A., Kits, K.D. and Stein, L.Y. (2016b) Comparison of nitrogen oxide metabolism
632 among diverse ammonia-oxidizing bacteria. *Frontiers Microbiol.* 7.

633 Laanbroek, H.J., Bodelier, P.L. and Gerards, S. (1994) Oxygen consumption kinetics of
634 Nitrosomonas europaea and Nitrobacter hamburgensis grown in mixed continuous cultures at
635 different oxygen concentrations. *Arch. Microbiol.* 161:156-162.

636 Laanbroek, H.J. and Gerards, S. (1993) Competition for limiting amounts of oxygen between
637 *Nitrosomonas europaea* and *Nitrobacter winogradskyi* grown in mixed continuous cultures.
638 Arch. Microbiol. 159:453-459.

639 Lehtovirta-Morley, L.E., Ross, J., Hink, L., Weber, E.B., Gubry-Rangin, C., Thion, C. *et al.*
640 (2016a) Isolation of '*Candidatus* Nitrosocosmicus franklandus', a novel ureolytic soil archaeal
641 ammonia oxidiser with tolerance to high ammonia concentration. FEMS Microbiol. Ecology
642 92:fiw057.

643 Lehtovirta-Morley, L. E., Sayavedra-Soto, L. A., Gallois, N., Schouten, S., Stein, L. Y., Prosser,
644 J. I., and Nicol, G. W. (2016b). Identifying Potential Mechanisms Enabling Acidophily in the
645 Ammonia-Oxidizing Archaeon "Candidatus Nitrosotalea devanaterra". *Applied and*
646 *environmental microbiology*, *82*(9), 2608-2619.

647 Löscher, C R., Kock, A., Könneke, M., LaRoche, J., Bange, H. W. and Schmitz, R.A. (2012)
648 Production of oceanic nitrous oxide by ammonia-oxidizing archaea. Biogeosci. 9:2419-2429.

649 Loveless, J.E. and Painter, H.A. (1968) The influence of metal ion concentrations and pH
650 value on the growth of a *Nitrosomonas* strain isolated from activated sludge. Microbiol. 52:1-
651 14.

652 Martens-Habbena, W., Berube, P.M., Urakawa, H., José, R. and Stahl, D. A. (2009) Ammonia
653 oxidation kinetics determine niche separation of nitrifying Archaea and Bacteria. Nature
654 461:976-979.

655 Martens-Habbena, W., Qin, W., Horak, R.E., Urakawa, H., Schauer, A. J., Moffett, J. W. *et al.*
656 (2015) The production of nitric oxide by marine ammonia-oxidizing archaea and inhibition of
657 archaeal ammonia oxidation by a nitric oxide scavenger. Environ. Microbiol. 17:2261-2274.

658 Molstad, L., Dörsch, P. and Bakken, L.R. (2007) Robotized incubation system for monitoring
659 gases (O_2, NO, N_2O, N_2) in denitrifying cultur*es. J. Microbiol. Meth.* 71:202-211.

660 Nadeem, S., Dörsch, P. and Bakken, L.R. (2013) Autoxidation and acetylene-accelerated
661 oxidation of NO in a 2-phase system: Implications for the expression of denitrification in *ex*
662 *situ* experiments. *Soil Biol. Biochem.* 57:606-614.

663 Norton, J.M., Klotz, M.G., Stein, L. Y., Arp, D.J., Bottomley, P.J., Chain, P.S., *et al.* (2008)
664 Complete genome sequence of *Nitrosospira multiformis*, an ammonia-oxidising bacterium
665 from the soil environment. Appl. Environ. Microbiol. 74:3559-3572.

666 Otten, M. F., Reijnders, W.N., Bedaux, J.J., Westerhoff, H.V., Krab, K. and Van Spanning, R.
667 J. (1999) The reduction state of the Q-pool regulates the electron flux through the branched
668 respiratory network of Paracoccus denitrificans. Eur. J. Biochem. 261:767-774.

669 Park S. and Bae W. (2009) Modelling the kinetics of ammonium oxidation and nitrite oxidation
670 under simultaneous inhibition by free ammonia and free nitrous oxide. Process Biochem.
671 44:631-640.

672 Qin, W., Meinhardt, K.A., Moffett, J.W., Devol, A.H., Virginia Armbrust, E., Ingalls, A.E. and
673 Stahl, D.A. (2017) Influence of oxygen availability on the activities of ammonia-oxidizing
674 archaea. Environ. Microbiol. Rep. 9:250-256.

675 Prosser, J.I. (1990) Autotrophic nitrification in bacteria. Adv. Microb. Physiol 30:125-181.

676 Remde, A. and Conrad, R. (1990) Production of nitric oxide in *Nitrosomonas europaea* by
677 reduction of nitrite. Archiv. Microbiol., 154:187-191.

678 Roco, C.A., Bergaust, L.L., Shapleigh, J.P. and Yavitt, J.B. (2016) Reduction of nitrate to nitrite
679 by microbes under oxic conditions. Soil Biol. Biochem.100:1-8.

680 Santoro, A.E., Buchwald, C., McIlvin, M.R. and Casciotti, K.L. (2011) Isotopic signature of N_2O
681 produced by marine ammonia-oxidizing archaea. Sci. 333:1282-1285.

682 Schmidt, I., Look, C., Bock, E. and Jetten, M.S. (2004) Ammonium and hydroxylamine uptake
683 and accumulation in *Nitrosomonas*. Microbiol. 150:1405-1412.

684 Simon, J. and Klotz, M.G. (2013) Diversity and evolution of bioenergetics systems involved in
685 microbial nitrogen compound transformations. Biochim. Biophys. Acta 1827:114-135.

686 Skinner, F.A. and Walker, N. (1961) Growth of *Nitrosomonas europaea* in batch and
687 continuous culture. Arch. Mikrobiol. 38:339-349.

688 Spang, A., Poehlein, A., Offre, P., Zumbrägel, S., Haider, S., Rychlik, *et al.* (2012) The genome
689 of the ammonia-oxidizing *Candidatus* Nitrososphaera gargensis: insights into metabolic
690 versatility and environmental adaptations. Environ. Microbiol. 14:3122-3145.

691 Splittgerber, A.G. (1983) Simplified treatment of two-substrate enzyme kinetics. J. Chem.
692 Educ. 60:651-655.

693 Stein, L.Y. (2011). Surveying N_2O-producing pathways in bacteria. Meth. Enzymol. 486:131–
694 152.

695 Stieglmeier, M., Mooshammer, M., Kitzler, B., Wanek, W., Zechmeister-Boltenstern, S.,
696 Richter, A. *et al*. (2014) Aerobic nitrous oxide production through N-nitrosating hybrid
697 formation in ammonia-oxidizing archaea. ISME J. 8:1135-1146.

698 Tourna, M., Stieglmeier, M., Spang, A., Könneke, M., Schintlmeister, A., Urich, T. *et al.* (2011)
699 *Nitrososphaera viennensis*, an ammonia oxidizing archaeon from soil. PNAS 108:8420-8425.

700 Vajrala, N., Martens-Habbena, W., Sayavedra-Soto, L.A., Schauer, A., Bottomley, P.J., Stahl,
701 D.A. *et al.* (2013) Hydroxylamine as an intermediate in ammonia oxidation by globally
702 abundant marine archaea. PNAS 110:1006-1011.

703 Walker, C.B., De La Torre, J.R., Klotz, M.G., Urakawa, H., Pinel, N., Arp, D.J., *et al.* (2010)
704 *Nitrosopumilus maritimus* genome reveals unique mechanisms for nitrification and autotrophy
705 in globally distributed marine crenarchaea. PNAS 107:8818-8823.

706 Whittaker, M., Bergman, D., Arciero, D. and Hooper, A.B. (2000) Electron transfer during the
707 oxidation of ammonia by the chemolithotrophic bacterium *Nitrosomonas europaea*. Biochim.
708 Biophys. Acta 1459:346-355.

709 Wrage, N., Velthof, G. L., Van Beusichem, M.L. and Oenema, O. (2001) Role of nitrifier
710 denitrification in the production of nitrous oxide. Soil Biol. Biochem. 33:1723-1732.

711 Yu, K. and Chandran, K. (2010) Strategies of *Nitrosomonas europaea* 19718 to counter low
712 dissolved oxygen and high nitrite concentrations. BMC Microbiol. 10:70

713 Zhu, X., Burger, M., Doane, T. A. and Horwath, W.R. (2013) Ammonia oxidation pathways
714 and nitrifier denitrification are significant sources of N_2O and NO under low oxygen availability.
715 PNAS 110:6328-6333.

716 Zhu-Barker, X., Cavazos, A.R., Ostrom, N.E., Horwath, W.R. and Glass, J.B. (2015) The
717 importance of abiotic reactions for nitrous oxide production. Biogeochem. 126:251-267.

718

Figure and Table legends

Figures

Fig. 1. Oxygen consumption kinetics (A - C), nitrite production (D - F) and nitrogen gas turnover (G - L) in 50-mL batch cultures contained in gas-tight serum bottles. Cultures of *N. europaea* (incubated with 4 mM TAN: A, D, G, J; incubated with 1 mM TAN: B, E, H, K) and *N. maritimus* (incubated with 1 mM TAN: C, F, I, L) were grown in mineral salts medium at a range of initial O_2 concentrations (see legend). O_2 was depleted entirely at low initial O_2 concentrations, while TAN rather than O_2 limited activity at high initial O_2 concentrations (A - C). NO_2^- concentration (D - F) is calculated on the basis of cumulative O_2 consumption and was similar to that measured (x) (Supporting Information Fig. S2). 1 nmol NO $vial^{-1}$ is equivalent to a concentration of 0.62 nM in the liquid. Means and standard errors of 3 - 5 replicate cultures are plotted.

Fig. 2. Oxygen- and TAN-dependent O_2 consumption rate by *N. europaea* (A, B) and *N. maritimus* (C, D) incubated with an initial TAN concentration of 1 mM. Three-dimensional plots (A, C) show cell-specific O_2 consumption rates (single time increment, individual vials) as a function of O_2 concentration at the cell surface ($[O_2]_s$; calculated from transport kinetics, see Experimental procedures) and the concentration of TAN. A double Michaelis-Menten equation (see Experimental procedures Eq. 4) was fitted to the data and is represented as a surface; measurements are shown as vertical lines from measurements to model values (red: measurement > model, blue: measurement < model). Two-dimensional plots (B, D) show the rates against O_2 concentrations for the 0.5 - 3% O_2 treatments at low ($[O_2]_s$, together with model estimates. Estimated kinetic parameters are shown in Table 1, and correlation between model estimates and measurements ($r^2 \geq 0.98$ for both strains) is shown in Supporting Information Fig. S5.

Fig. 3. Cell-specific rates of NO and N_2O production by *N. europaea* (A, C) and *N. maritimus* (B, D) incubated with an initial TAN concentration of 1 mM. The rate of NO

production (V_{NO}) (A, B) is corrected for NO autoxidation and reflects enzymatic production (positive values) and consumption (negative values). Cultures depleted either O_2 and/or TAN entirely, depending on the initial O_2 concentration in the headspace (see legend). Limitation of O_2 and/or TAN also affected the rate of N_2O production (C, D).

Fig. 4. Relationship between velocity of N_2O (V_{N2O}) production and O_2 consumption rates (V_{O2}) of *N. europaea* (A) and *N. maritimus* (B) incubated with 1 mM TAN at a range of initial O_2 concentrations (see legend).

Fig. 5. Oxygen-dependent N_2O yield of *N. europaea* (incubated with 1 mM TAN, A, or with 4 mM TAN, B) and *N. maritimus* (incubated with 1 mM TAN, C). N_2O yield is expressed as N_2O-N per NO_2^--N generated from ammonia oxidation in cultures incubated with a range of initial O_2 concentrations (see legend).

Fig. 6. Electron flow to denitrification (amol e^- $cell^{-1}$ h^{-1}) for *N. europaea* growing on 1 mM TAN; model predictions versus measurements. The electron flow rate to nitrifier denitrification (V_{eD}) are based on measurements (NO and N_2O concentration) of single time increment values. Model predictions are plotted as continuous lines, using the experimentally determined concentrations of ($[O_2]_s$ and [TAN] as inputs (average values for replicate vials at each time point). The insert highlights the declining electron flow to nitrifier denitrification at very low ($[O_2]_s$ concentration and the failure of the model to capture this phenomenon. The model parameters (see Supporting Information, "Modelling electron flow in *N. europaea* grown at 1 mM TAN") are Y_{HAO} = 0.0019 (proportion of oxidised hydroxylamine-N released as N_2O-N), k_{mO2} = 11.2 µM O_2 (half-saturation concentration for terminal oxidases), V_{maxeTO} = 640 x V_{maxeD} (V_{maxeTO} and V_{maxeD} are the maximum rates of electron flow to terminal oxidases and denitrification, respectively).

Fig. 7. Simplified electron flow in *N. europaea*. The 4 electrons per NO_2^- produced by hydroxylamine dehydrogenase (HAO) are relayed to the quinone pool (Q) most plausibly via membrane cytochrome c_{m552}, or via periplasmic C_{554} and C_{m552} (see discussion by Simon and

Klotz, 2013). Ammonia monooxygenase (AMO) draws 2 electrons from the quinone pool and the remaining 2 electrons are passed either to NAD (-> NADH, reducing power for CO_2 assimilation) or to periplasmic cytochrome C_{552} via the cytochrome bc1 complex. C_{552} is a branching point, delivering electrons either to terminal oxidases (TO) or to the denitrification enzymes (D), i.e. nitrite reductase and nitric oxide reductase (nirK and NorB, Arp and Stein, 2003). Several different C_{552} proteins may be involved at this branching point (Klotz and Stein, 2010). Our modelling of competition for electrons (TO versus D) assuming one common electron donor is therefore a gross simplification. Proton motive force is generated by *bc1* and TO (Klotz and Stein, 2008; Kozlowski et al., 2016a), while the electron transport from HAO to Q may be electroneutral (Simon and Klotz, 2013). An electron shunt from c_{554} to C_{552} is indicated (red dashed arrow), which has been suggested by Stein *et al.* (2013) as an electron neutral pathway to D.

Table legend.

Table 1. Estimated kinetic parameters for O_2 consumption as a function of O_2 and TAN concentration in *N. europaea* and *N. maritimus.*

Tables and Figures:

Table 1. **Estimated kinetic parameters for O_2 consumption rate as a function of O_2 and TAN concentration in *N. europaea* and *N. maritimus*.**

	V_{max}[§] (fmol O_2 $cell^{-1}$ h^{-1})	k_{O2}[§] (µM O_2)	k_{TAN}[§] (mM TAN)
N. europaea	17.6 (0.6) [15.6-17.9]	2.35 (0.13) [2.2-2.6]	0.565 (0.04) [0.44-0.59]
N. maritimus	1.0 (0.01) [0.98-1.03]	2.13 (0.08) [2.0-2.3]	0.20 (0.02) [0.18-0.23]

[§] Kinetic parameters were estimated from cultures that were incubated with an initial TAN concentration of 1 mM and a range of O_2 concentrations. The dataset for each strain was fitted with Eq. 4. Standard deviations are displayed in parentheses and 95% confidence intervals in brackets.

Fig. 1

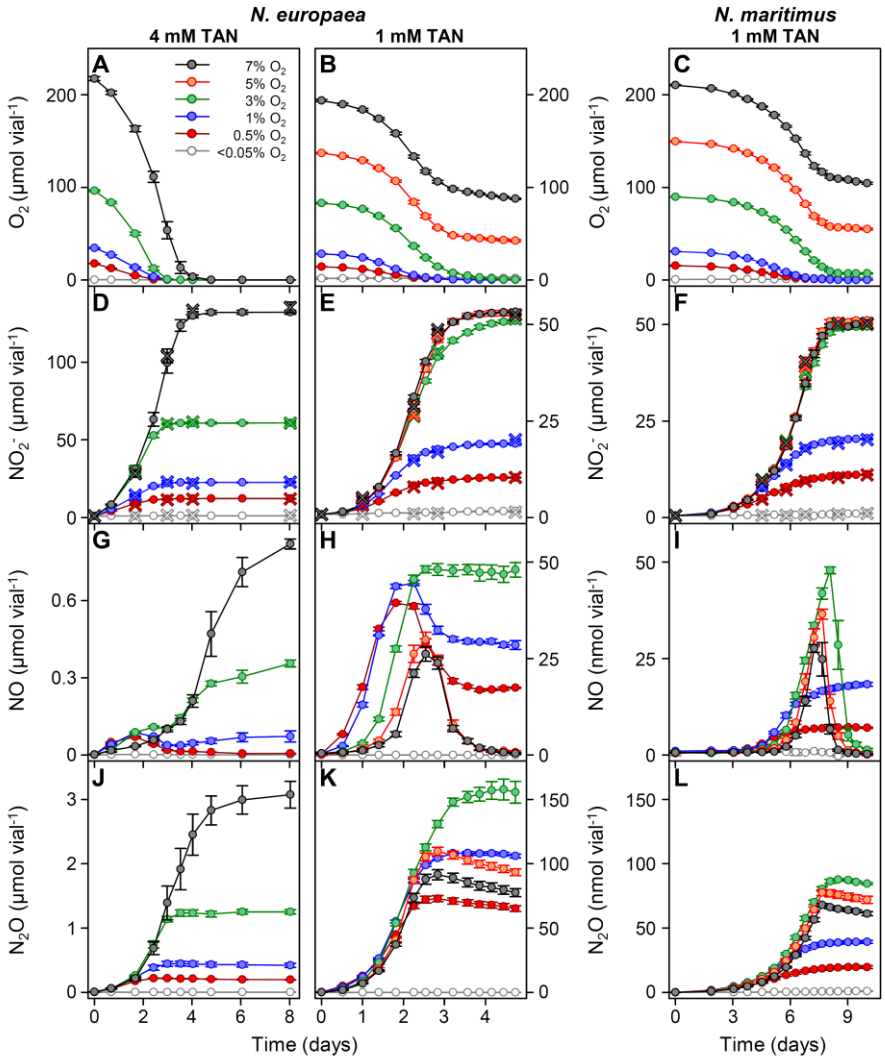

Fig. 1. Oxygen consumption kinetics (A - C), nitrite production (D - F) and nitrogen gas turnover (G - L) in 50-mL batch cultures contained in gas-tight serum bottles. Cultures of *N. europaea* (incubated with 4 mM TAN: A, D, G, J; incubated with 1 mM TAN: B, E, H, K) and *N. maritimus* (incubated with 1 mM TAN: C, F, I, L) were grown in mineral salts medium at a range of initial O_2 concentrations (see legend). O_2 was depleted entirely at low initial O_2 concentrations, while TAN rather than O_2 limited activity at high initial O_2 concentrations (A - C). NO_2^- concentration (D - F) is calculated on the basis of cumulative O_2 consumption and was similar to that measured (x) (Supporting Information Fig. S2). 1 nmol NO $vial^{-1}$ is equivalent to a concentration of 0.62 nM in the liquid. Means and standard errors of 3 - 5 replicate cultures are plotted.

Fig. 2

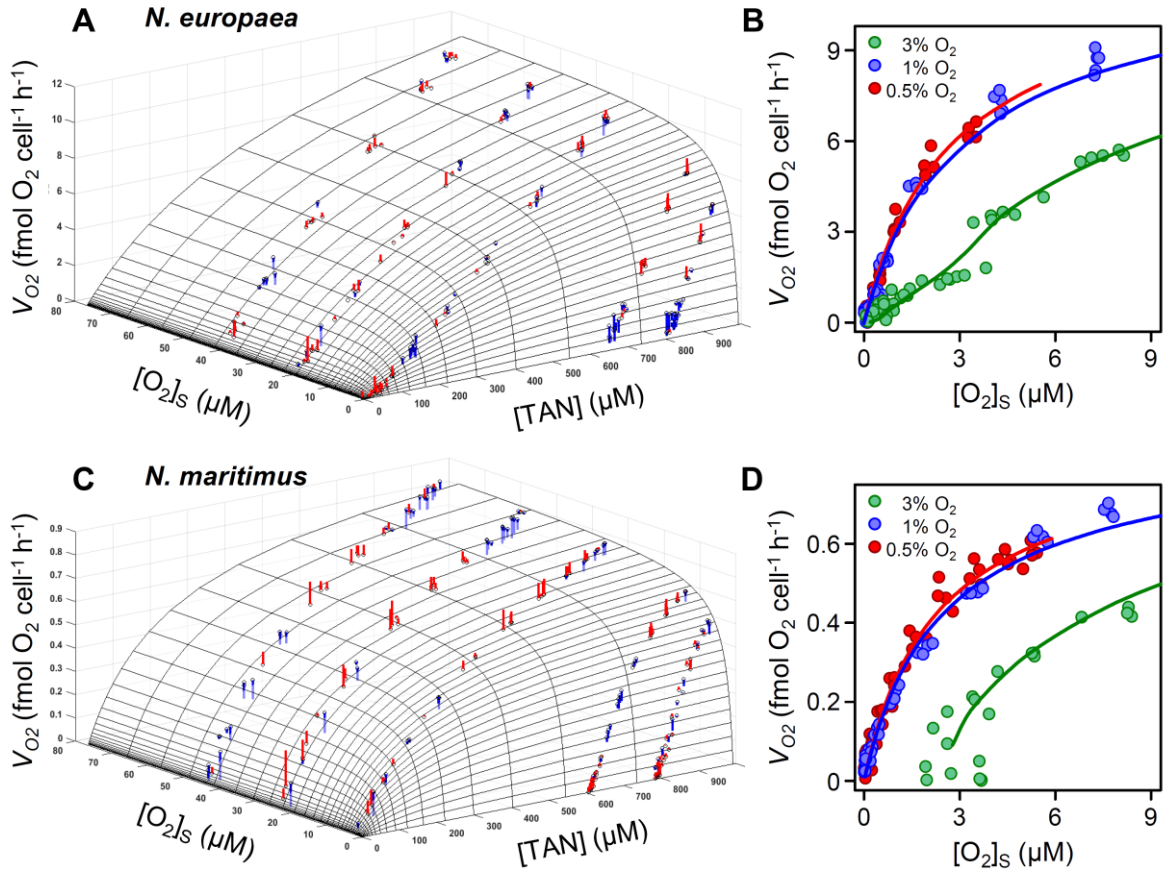

Fig. 2. Oxygen- and TAN-dependent O_2 consumption rate by *N. europaea* (A, B) and *N. maritimus* (C, D) incubated with an initial TAN concentration of 1 mM. Three-dimensional plots (A, C) show cell-specific O_2 consumption rates (single time increment, individual vials) as a function of O_2 concentration at the cell surface ($[O_2]_s$; calculated from transport kinetics, see Experimental procedures) and the concentration of TAN. A double Michaelis-Menten equation (see Experimental procedures Eq. 4) was fitted to the data and is represented as a surface; measurements are shown as vertical lines from measurements to model values (red: measurement > model, blue: measurement < model). Two-dimensional plots (B, D) show the rates against O_2 concentrations for the 0.5 - 3% O_2 treatments at low ($[O_2]_s$, together with model estimates. Estimated kinetic parameters are shown in Table 1, and correlation between model estimates and measurements (r^2≥0.98 for both strains) is shown in Supporting Information Fig. S5.

Fig. 3

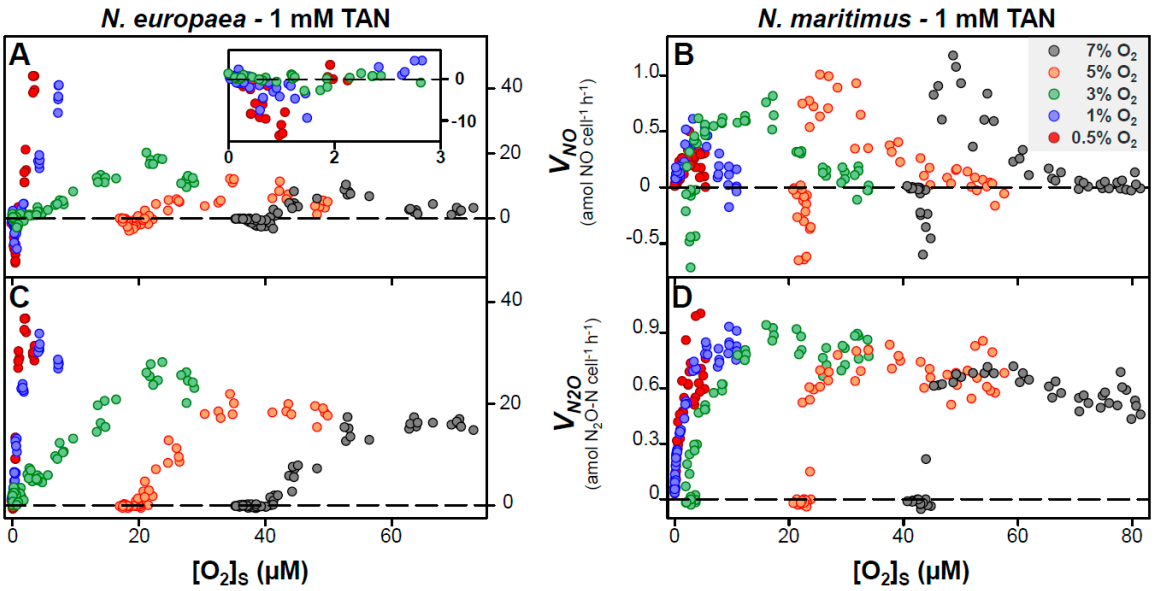

Fig. 3. Cell-specific rates of NO and N_2O production by *N. europaea* (A, C) and *N. maritimus* (B, D) incubated with an initial TAN concentration of 1 mM. The rate of NO production (V_{NO}) (A, B) is corrected for NO autoxidation and reflects enzymatic production (positive values) and consumption (negative values). Cultures depleted either O_2 and/or TAN entirely, depending on the initial O_2 concentration in the headspace (see legend). Limitation of O_2 and/or TAN also affected the rate of N_2O production (C, D).

Fig. 4

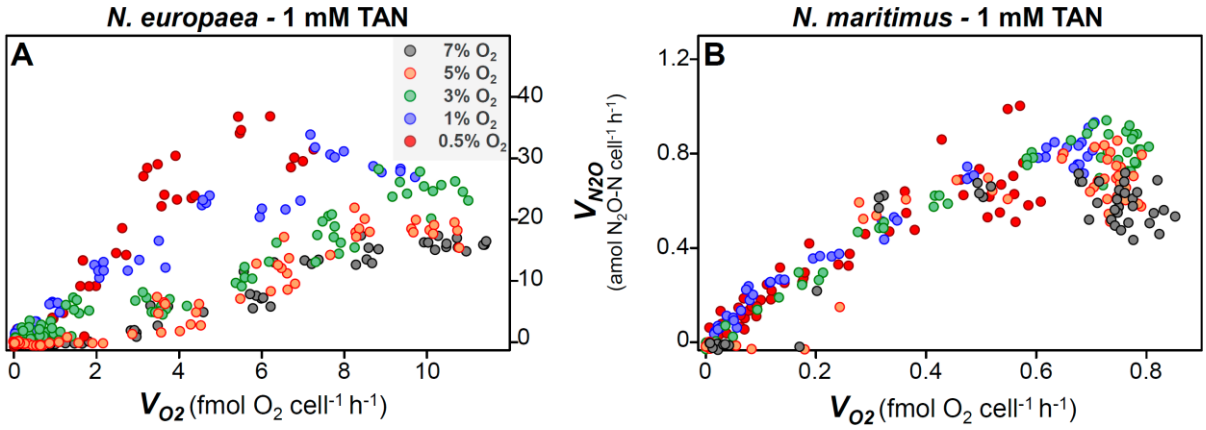

Fig. 4. Relationship between velocity of N_2O (V_{N2O}) production and O_2 consumption rates (V_{O2}) of *N. europaea* (A) and *N. maritimus* (B) incubated with 1 mM TAN at a range of initial O_2 concentrations (see legend).

Fig. 5

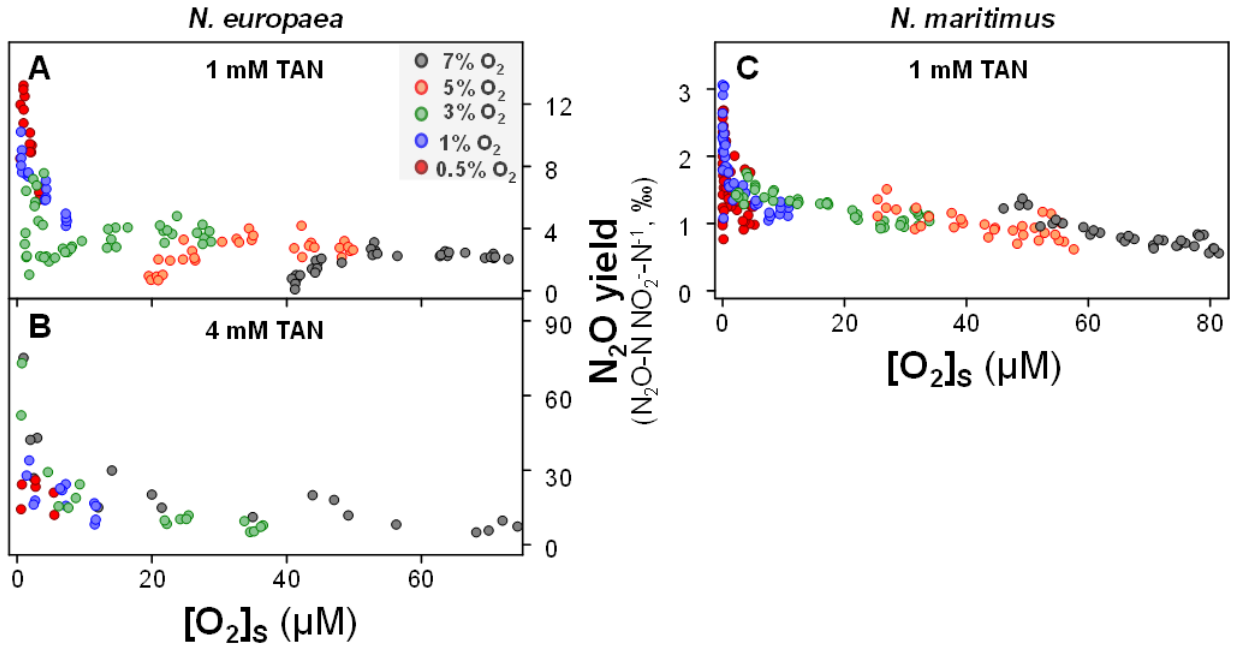

Fig. 5. Oxygen-dependent N_2O yield of *N. europaea* (incubated with 1 mM TAN, A, or with 4 mM TAN, B) and *N. maritimus* (incubated with 1 mM TAN, C). N_2O yield is expressed as N_2O-N per NO_2^--N generated from ammonia oxidation in cultures incubated with a range of initial O_2 concentrations (see legend).

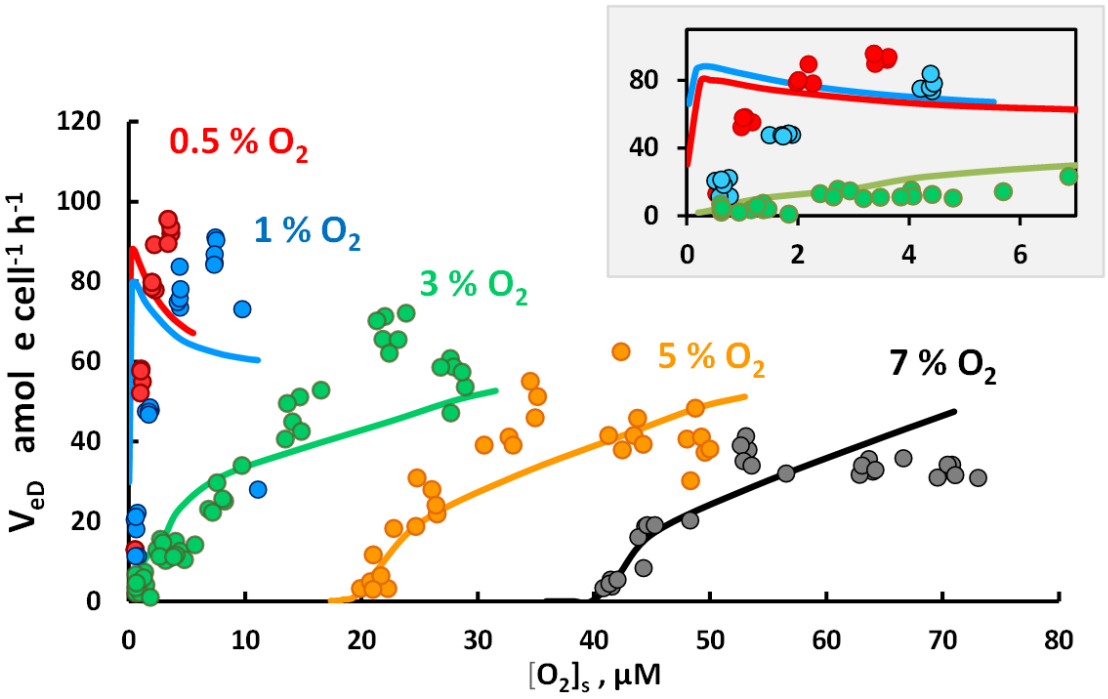

Fig. 6. Electron flow to denitrification (amol e^- $cell^{-1}$ h^{-1}) for *N. europaea* growing on 1 mM TAN; model predictions versus measurements. The electron flow rate to nitrifier denitrification (V_{eD}) are based on measurements (NO and N_2O concentration) of single time increment values. Model predictions are plotted as continuous lines, using the experimentally determined concentrations of ($[O_2]_s$ and [TAN] as inputs (average values for replicate vials at each time point). The insert highlights the declining electron flow to nitrifier denitrification at very low ($[O_2]_s$ concentration and the failure of the model to capture this phenomenon. The model parameters (see Supporting Information, "Modelling electron flow in *N. europaea* grown at 1 mM TAN") are Y_{HAO} = 0.0019 (proportion of oxidised hydroxylamine-N released as N_2O-N), k_{mO2} = 11.2 µM O_2 (half-saturation concentration for terminal oxidases), V_{maxeTO} = 640 x V_{maxeD} (V_{maxeTO} and V_{maxeD} are the maximum rates of electron flow to terminal oxidases and denitrification, respectively).

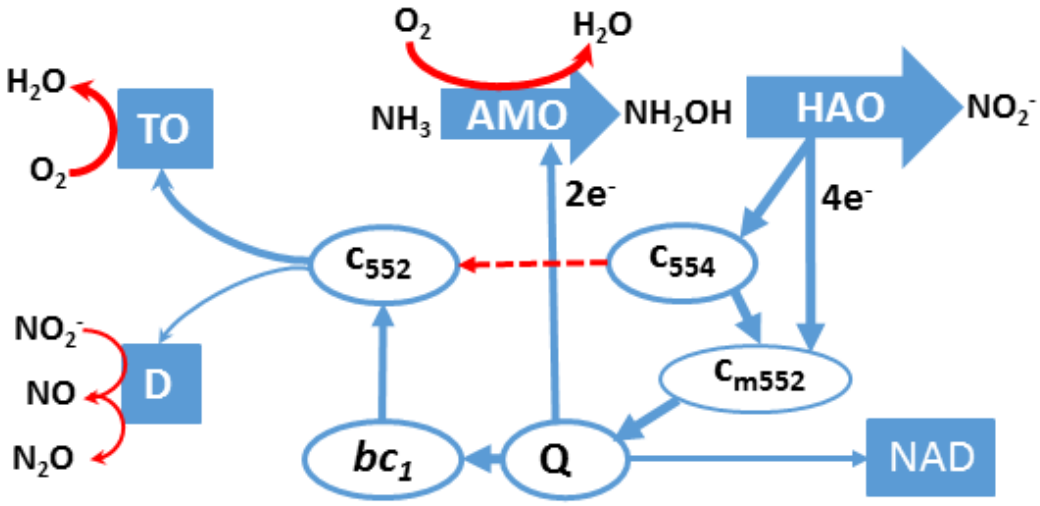

Fig. 7. Simplified electron flow in *N. europaea*. The 4 electrons per NO_2^- produced by hydroxylamine dehydrogenase (HAO) are relayed to the quinone pool (Q) most plausibly via membrane cytochrome c_{m552}, or via periplasmic C_{554} and C_{m552} (see discussion by Simon and Klotz, 2013). Ammonia monooxygenase (AMO) draws 2 electrons from the quinone pool and the remaining 2 electrons are passed either to NAD (-> NADH, reducing power for CO_2 assimilation) or to periplasmic cytochrome C_{552} via the cytochrome bc1 complex. C_{552} is a branching point, delivering electrons either to terminal oxidases (TO) or to the denitrification enzymes (D), i.e. nitrite reductase and nitric oxide reductase (nirK and NorB, Arp and Stein, 2003). Several different C_{552} proteins may be involved at this branching point (Klotz and Stein, 2010). Our modelling of competition for electrons (TO versus D) assuming one common electron donor is therefore a gross simplification. Proton motive force is generated by *bc1* and TO (Klotz and Stein, 2008; Kozlowski et al., 2016a), while the electron transport from HAO to Q may be electroneutral (Simon and Klotz, 2013). An electron shunt from c_{554} to C_{552} is indicated (red dashed arrow), which has been suggested by Stein *et al.* (2013) as an electron neutral pathway to D.

Supporting information

Contents

1. Figures and Table

2. Modelling electron flow in *N. europaea* grown at 1 mM TAN

3. Modelling electron flow in *N. europaea* grown at 4 mM TAN

1. Figures and Table

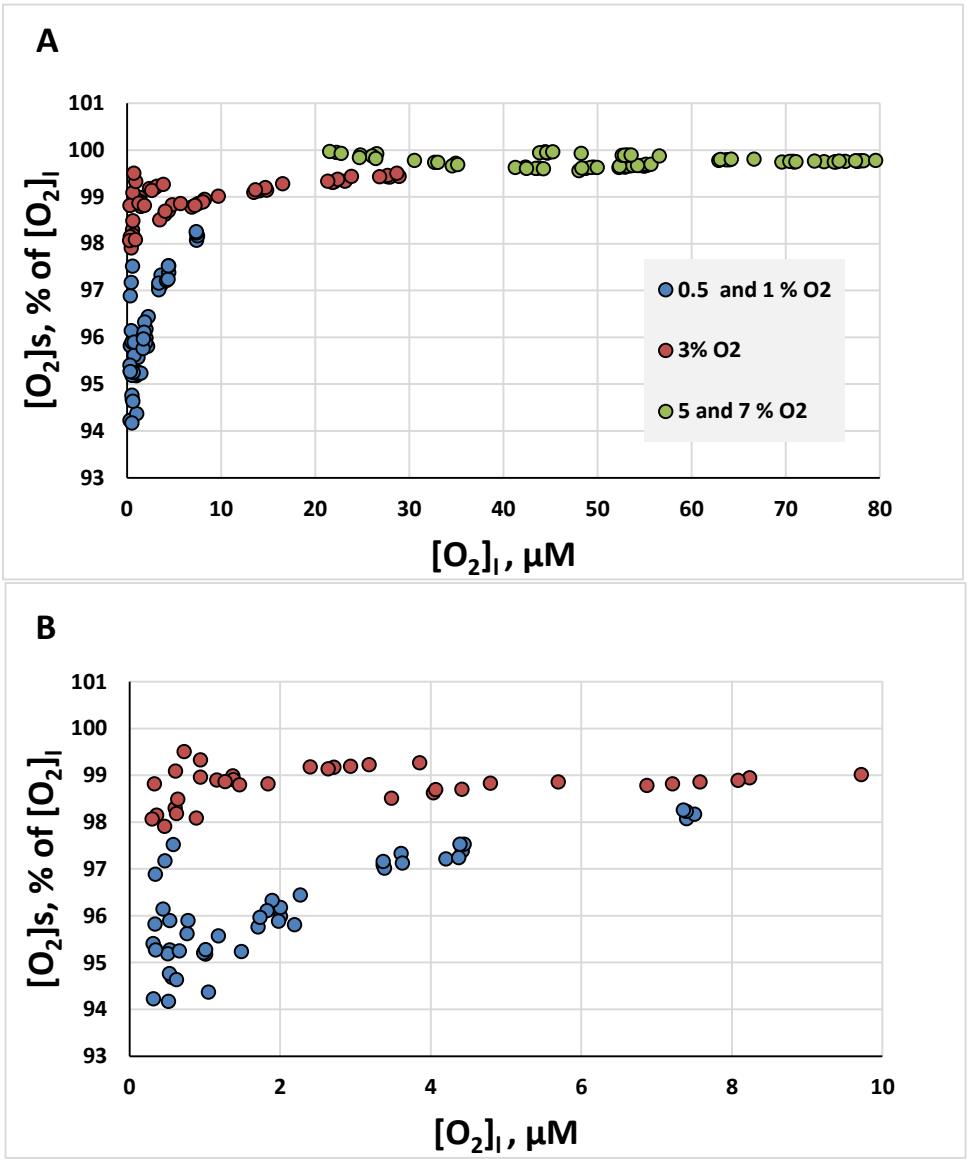

Fig. S1. Oxygen concentration at the cell surface of *Nitrosomonas europaea* as a function of O_2 concentration in the bulk liquid and the flux. Estimated cell surface concentration of O_2 ($[O_2]_s$) and in the bulk liquid [($[O2]_l$) were calculated from the observed cell-specific O_2 consumption rates in batch cultures with 1 mM TAN incubated at different initial O_2 concentrations (see legend). Single time increment values are plotted. Panel A: entire $[O_2]_l$ range, panel B: concentration range 0-10 µM. In the vials with initially containing 0.5 and 1% O_2, TAN was not depleted, and the only limitation of O_2 consumption was the concentration of O_2. In these treatments, $[O_2]_s$ declined towards 95% of $[O_2]_l$ at low concentrations. In the 3% O_2 treatment, TAN and O_2 were depleted at approximately the same time. Thus cell-specific O_2 consumption became limited by both and, as a result, $[O_2]_S$ remained similar to $[O_2]_l$, even at very low oxygen concentrations.

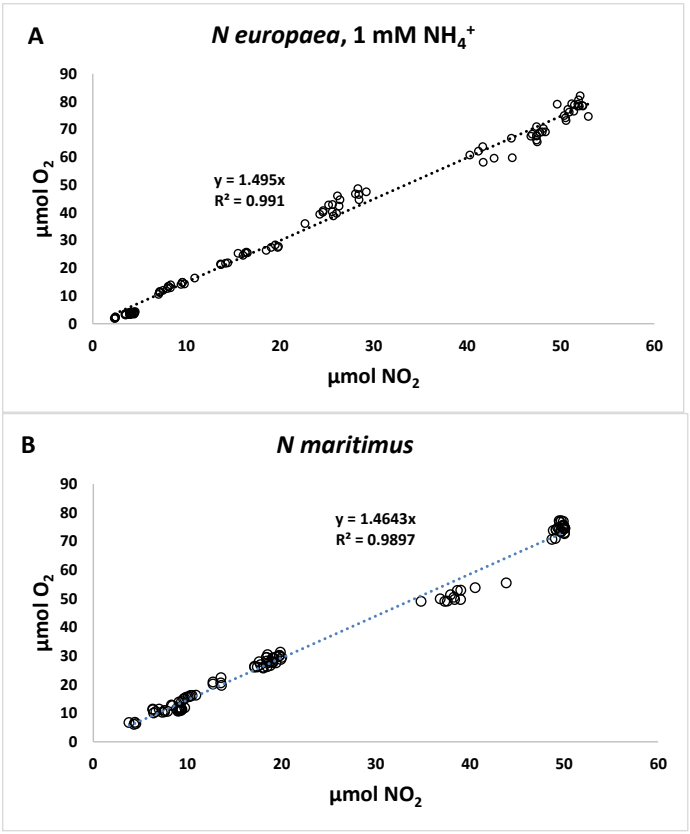

Fig. S2. Relationship between cumulated O_2 consumption and NO_2^- production. *N. europaea* batches with 1 mM TAN (A), *N. maritimus* 1 mM TAN (B). Estimated linear regression functions are shown. The 95% confidence intervals of regression coefficients are [1.48; 1.52] for *N. europaea* and [1.44; 1.50] for *N. maritimus*.

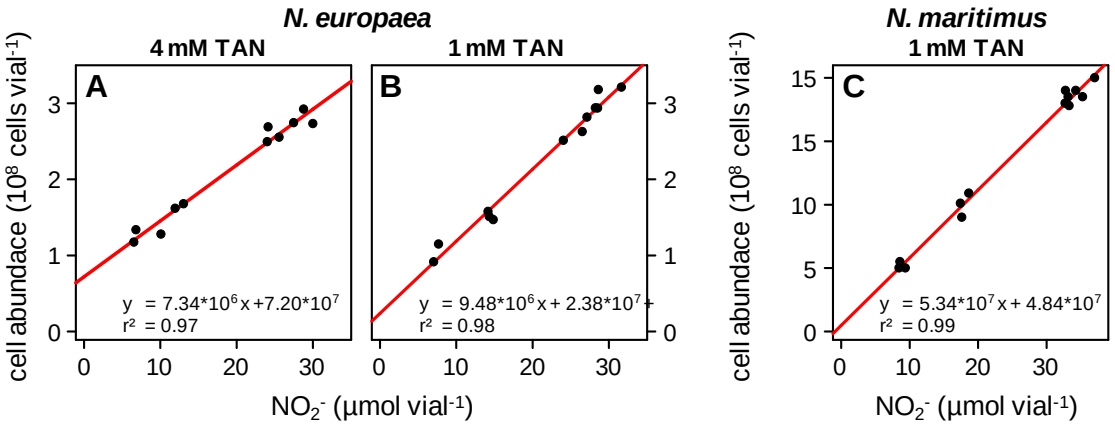

Fig. S3. Relationship between cell abundance and NO_2^- production. Cell abundance of *N. europaea* batch cultures with 4 mM TAN (A), *N. europaea* cultures with 1 mM TAN (B) and *N. maritimus* cultures with 1 mM TAN (C) when cultures were in mid-exponential phase was determined by enumeration of DAPI-stained cells using epifluorescence microscopy. The slope of each regression (solid red line) indicates the cell yield (cells µmol $NO_2^{-\,-1}$ $vial^{-1}$) and the intercept the initial cell abundance. The fit of each regression is indicated by r^2 values.

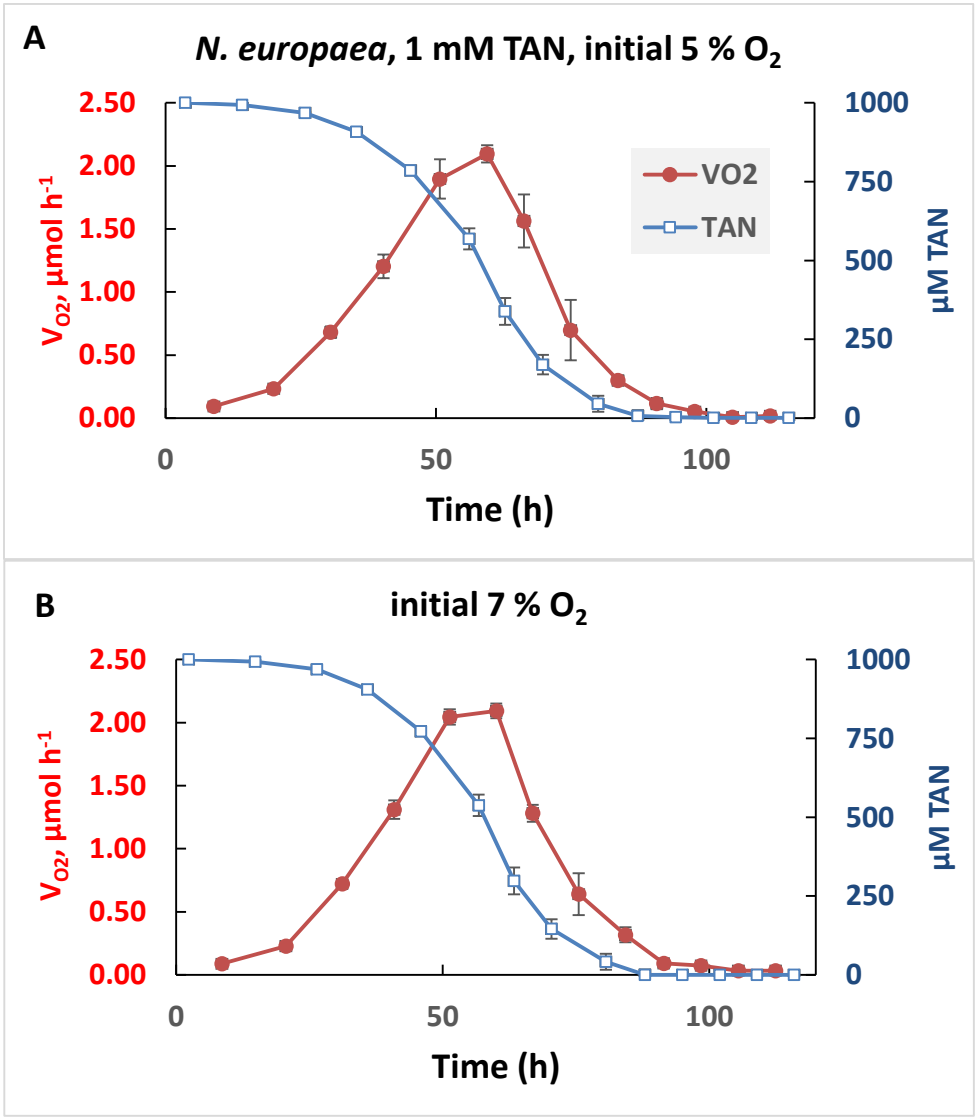

Fig. S4. Oxygen consumption rates in the *Nitrosomonas europaea* batch cultures in response to TAN-depletion. Results for vials with 1 mM TAN and initially 5% (A) and 7% O_2 (B) in the headspace. The panels show O_2 consumption rates (red , left axis) for each time increment; and the concentration of TAN (blue, right axis); demonstrating that the oxygen consumption rate decline towards zero in response to TAN depletion. The same is true for *N. maritimus* (5 and 7% O_2 treatments) after depletion of 1 mM TAN around 200 h after inoculation (result not shown).

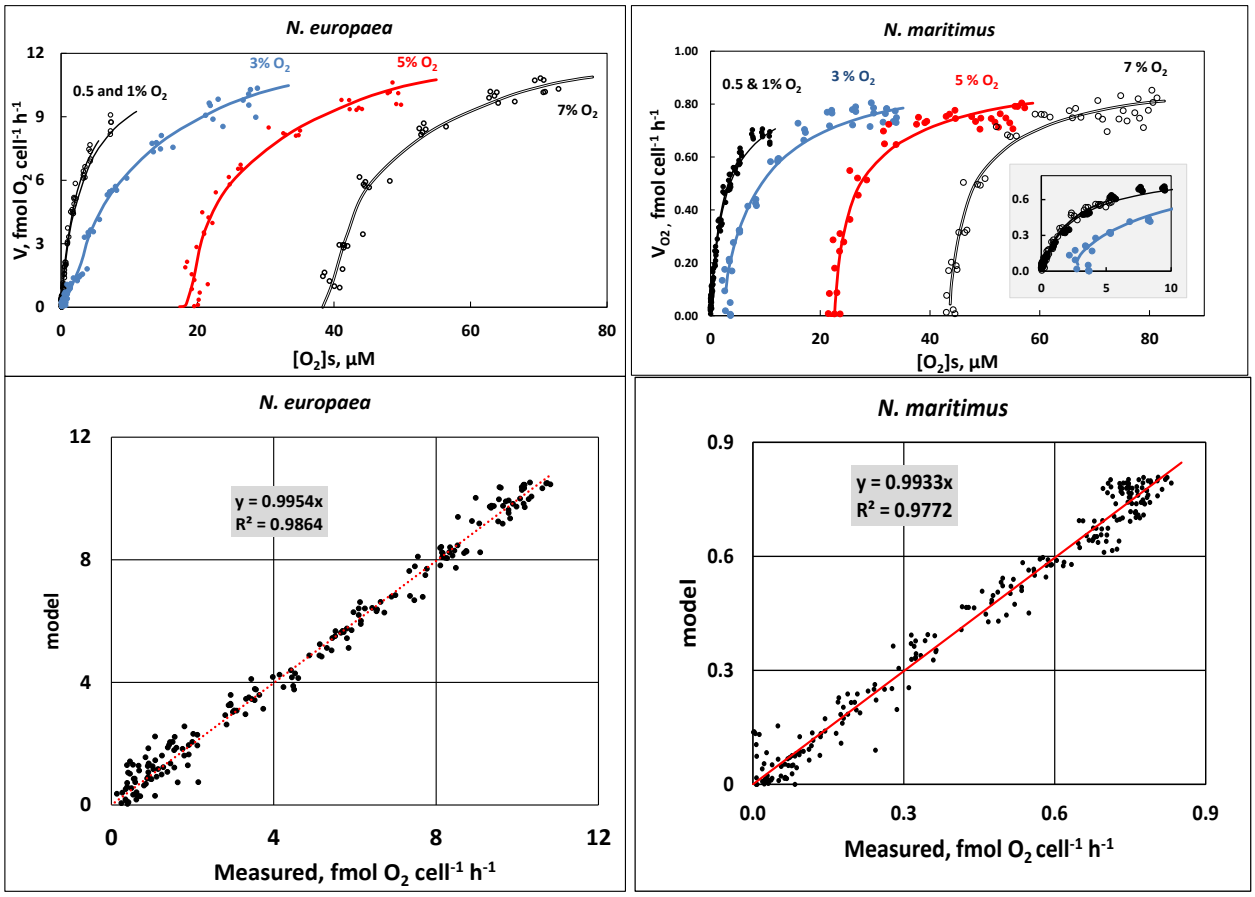

Fig. S5. Evaluation of model fit for the enzyme kinetic model of cell-specific O_2 consumption as a function of TAN concentration and the concentration of O_2 at the cell surface. *The upper panels show cell-specific O_2 consumption (V_{O2}) of N. europaea and N. maritimus batch cultures with 1 mM TAN, with various initial O_2 concentrations (indicated in panels) against O_2 concentration at cell surface, and model predictions (continuous lines). The lower panels show model predictions versus measured values for V_{O2} (fmol O_2 cell^{-1} h^{-1}) with regression functions..*

Table S1. Growth kinetics, oxygen consumption rate, and growth yield in the 7% O_2 treatment of *N. europaea* batch cultures with 1 and 4 mM TAN and *N. maritimus* batch cultures with 1 mM TAN.

		Growth rate[$] ($h^{-1}$)	V_{O2}[#] (fmol $cell^{-1}$ h^{-1})	Growth yield[§] (cells mol^{-1} NO_2^-)
N. europaea **1 mM TAN**		0.045	6.87	**9.48×10^{12}**
		0.044	6.98	
		0.045	7.05	
		0.044	6.91	
		0.042	6.63	
	Average	**0.044**	**6.88**	
	Std. dev.	**0.001**	**0.14**	
N. europaea **4 mM TAN**		0.036	7.60	**7.34×10^{12}**
		0.032	5.55	
		0.035	6.97	
	Average	**0.034**	**6.71**	
	Std. dev.	**0.002**	**1.05**	
N. maritimus **1 mM TAN**		0.030	0.71	**5.43×10^{13}**
		0.027	0.74	
		0.027	0.76	
		0.027	0.76	
		0.028	0.77	
	Average	**0.028**	**0.75**	
	Std. dev.	**0.001**	**0.02**	

[$]Growth rate of each replicate vial was estimated by nonlinear regression of cell abundance against time for the time period when O_2 was not limiting (NO_2^- increasing exponentially).

[#]V_{O2} of each replicate vial was estimated from the average for the time period for which growth rate was determined.

[§]Average growth yield was estimated by regression of cell numbers against NO_2^- production (Fig. S3).

[&]ANOVA of V_{O2} and growth rates show that *N. europaea* grew significantly ($p<0.001$) faster at 1 than at 4 mM TAN, but the cell-specific O_2 consumption rates at the two ammonium concentrations were not significantly different ($p=0.76$).

2. Modelling electron flow in *Nitrosomonas europaea* grown at 1 mM TAN

The experiment showed that the yield of N_2O, Y_{N2O} (‰ of N_2O-N per NO_2^--N generated from NH_3-N oxidised) increased with declining O_2 concentration. This was expected because it is believed that there are two pathways (at least) for N_2O production:

1. Incomplete hydroxylamine oxidation (or reaction of hydroxylamine with other intermediates such NO or NO_2^-), releasing a small but constant fraction of oxidised N as N_2O
2. Respiratory driven NO and N_2O production (nitrifier denitrification), once the respiration of oxygen becomes concentration limited.

This was modelled using the following assumptions.

1. A constant fraction of the oxidised ammonia is released as N_2O (and possibly NO), independent of the O_2 concentration (pathway 1 above).
2. Constitutively expressed denitrification enzymes (D), nitrite and nitric oxide reductase are inactive at full aeration, because the terminal oxidases (TO) compete strongly for electrons. However, when limited by low O_2 concentrations, TO's ability to compete for electrons is reduced and an increasing fraction of electrons are passed over to D.
3. The kinetics of this nitrifier denitrification were based on estimated steady state flows of electrons through the most relevant flow paths as a function of O_2 concentration. Fig 7 (main paper) illustrates the relevant electron pathways involved, and the stoichiometry, based on Whittaker *et al*. (2000). Two of the 4 electrons from HAO are channelled to AMO to drive the consumption of 1 molecule O_2 per molecule NH_3 oxidised to hydroxylamine. The remaining two electrons are either channelled to terminal oxidases or to the reverse electron transfer pathway to produce NAD(P)H. If both electrons are transferred to terminal oxidases, the O_2 consumption would be 0.5 mol O_2 mol^{-1} NO_2^- produced. Hence the overall stoichiometry would be $NH_3 + 1.5\ O_2 \rightarrow NO_2^- + H^+ + H_2O$ (Whittaker *et al*., 2000).

   Model of the electron flow, as determined by the concentration of O_2

   Terminal oxidases can be assumed to exist in excess (electron flow never reaching V_{max}). Thus, the potential electron flow rate to TO or denitrification enzymes D (if oxygen concentration is not limiting) is a linear function of the rate of ammonia oxidation

   $$V_{eR} = V_{eamox} * f_{eR} \quad (1)$$

   where

   - V_{eR} is the electron flow rate to terminal oxidases or denitrification enzymes (via C_{552}), driven by V_{eamox}
   - V_{eamox} is the net electron flow from ammonia- and hydroxylamine-oxidation (2 mol per mol O_2)
   - f_{eR} is the fraction of electrons directed to terminal oxidases or denitrification enzymes, at low O_2 concentrations (the fraction directed to NAD is $1-f_{eR}$).

V_{eR} is assumed to be partitioned between TO and D, depending on the oxygen concentration; the two terminal electron acceptor pathways are assumed to compete for the electrons:

$$V_{eR} = V_{eD} + V_{eTO} \quad (2)$$

where

- V_{eD} is the electron flow to D
- V_{eTO} is the electron flow to TO
- TO and D compete for electrons from c_{552} and this competition depends on their affinity for c_{552}, but also on the availability of their terminal electron acceptors. To simplify, nitrite and nitric oxide reductase are combined and the two electron flows depend on the concentration of reduced cytochrome c_{552} (denoted as $[c^*_{552}]$) and the concentrations of the terminal electron acceptors:

$$V_{eD} = V_{maxeD} \frac{[c^*_{552}]}{c^*_{552} + k_{mD}} * \frac{[NO_2^-]}{[NO_2^-] + k_{mNO2}} \quad (3)$$

$$V_{eTO} = V_{maxeTO} \frac{[c^*_{552}]}{c^*_{552} + k_{mTO}} * \frac{[O_2]}{[O_2] + k_{mO2}} \quad (4)$$

Where

- V_{maxeD} is the maximum rate of electron flow to NO_2^- and NO via D
- k_{mD} is the half-saturation constant describing the affinity of the N-reductases to c^*_{552}
- $[NO_2^-]$ is the concentration of NO_2^-
- k_{mNO2} is the half-saturation constant describing the affinity of nitrite reductase to NO_2^-
- V_{maxeTO} is the maximum electron flow to O_2 via TO
- k_{mTO} is the half-saturation constant describing the affinity of TO to c^*_{552}
- $[O_2]$ is the concentration of O_2
- k_{mO2} is the half-saturation constant describing the affinity of TO to O_2

As the model describes situations where $[NO_2^-] >> k_{mNO2}$, the term $\{[NO_2^-]/([NO_2^-] + k_{mNO2})\}$ is ~1, and equation 3 can be simplified:

$$V_{eD} = V_{maxeD} \frac{[c^*_{552}]}{c^*_{552} + k_{mD}} \quad (5)$$

Equation 5 implies that $[c^*_{552}]$ can be assumed to reach steady state depending on the concentration of electron transfer to D and TO and the rate of electrons passed from *bc1*, which we assume to be constant for a given concentration of TAN:

$$\frac{d[C^*_{552}]}{dt} = V_{eR} - V_{eTO} - V_{eD} \quad (6)$$

where V_{eR} is the electron flow from *bc1* to c_{552} (assumed to be determined by the concentrations of TAN and O_2, implicitly assuming that ammonium monooxygenase is the rate liming enzyme).

Thus, for any given V_{eR} and concentration of O_2, the steady state [c^*_{552}] can be found by numeric simulation and the ratio between V_{eD} and V_{eTO} at steady state is given by

$$\frac{V_{eD}}{V_{eTO}} = \frac{V_{maxeD}\frac{[c^*_{552}]}{[c^*_{552}]+k_{mD}}}{V_{maxeTO}\left(\frac{[O_2]}{[O_2]+k_{mO2}}\right)\left(\frac{[c^*_{552}]}{[c^*_{552}]+k_{mTO}}\right)} \qquad (7)$$

At steady state, d[c^*_{552}]/dt = 0, hence $V_{eR} = V_{eD} + V_{eTO}$. Following algebraic manipulation, the proportion of total electron flow to respiratory metabolism (V_{eR}) which is passed to denitrification enzymes is given by equation 8:

$$\frac{V_{eD}}{V_{eR}} = \left(1 + \frac{\frac{V_{maxeTO}}{[c^*_{552}]+k_{TO}} * \frac{[O_2]}{[O_2]+k_{mO2}}}{\frac{V_{maxeD}}{[c^*_{552}]+k_D}}\right)^{-1} \qquad (8)$$

Equation 8 includes the concentration of c^*_{552}, hence requiring that this concentration is found by numerical simulation to determine steady state [c^*_{552}] for a given concentration of O_2 and V_{eR}; the latter is also a function of O_2 concentration, and can be predicted from the empirically parameterised double Michaelis-Menten equation for-whole cell O_2 consumption (as equation 4 in main text):

$$V_{O_2} = V_{max} * \frac{[O_2]_S}{[O_2]_S+k_{mO_2}} \frac{[TAN]}{[TAN]+k_{mTAN}} \quad (9)$$

The parameter values used were V_{max} = 17.6 fmol O_2 cell^{-1} h^{-1}, k_{mO2} = 2.35 µM O_2, k_{mTAN} = 567 µM TAN, taken from Table 1 (main text).

To find the steady state [c^*_{552}], an initial (arbitrary) concentration is set and then changed according to equations 5, 6 and 7, given the concentrations of O_2 and TAN (the latter predicting V_{eR}). Steady state [C^*_{552}] is reached within minutes.

If, however, k_{mTO} and k_{mD} are assumed to be equal (i.e. the kinetics of the two enzyme reactions only differ in their V_{max} values), the [C^*_{552}] can be eliminated from equation 8, and the predicted ratio V_{eD}/V_{eR} is given by equation 10:

$$\frac{V_{eD}}{V_{eR}} = \left(1 + \frac{V_{maxTO}}{V_{maxD}} * \frac{[O_2]}{[O_2]+k_{mO2}}\right)^{-1} \qquad (10)$$

As stated above, the implicit assumption in equation 10 is that competition for electrons from c^*_{552} between TO and D only depends on their V_{max} (affinity is assumed to be the same for the two enzyme systems).

Experimental data include NO and N_2O from the denitrification pathway plus the commonly hypothesised N_2O production via incomplete oxidation of hydroxylamine, which is assumed to be a constant fraction of ammonia oxidation (Y_{HAO}). Since we have combined nitrite and nitric oxide reductases, the model provides no prediction of the product stoichiometry (NO/N_2O), only the electron flow to denitrification and the N_2O production from HAO.

Parameter estimations, assuming identical affinity for C_{552}

The dataset used to estimate the parameters were the 1 mM TAN experiment with *N. europaea* and the estimated parameters for O_2 consumption kinetics given in Table 1 (main text) were adopted to predict V_{eR} as a function of O_2 and TAN concentrations, using equation 9.

Since V_{O2} in this equation is the sum of O_2 consumption by ammonium monooxygenase and TO, $V_{eR} = V_{O2*}1.33$. The fraction of electrons directed to terminal oxidases (f_{eR} , equation (1)) is unknown, but it appears to be very close to 1, considering the stoichiometry observed (the organisms consumed close to 1.5 mol O_2 per mol NO_2^- produced (Fig S 2). Based on the observed growth yield per mol NO_2^- (Table S1), we reach the same conclusion: The necessary reducing power to support this growth amounts to less than 5% of the electron flow from ammonium- and hydroxylamine oxidation. Thus, we used f_{eR}=0.95.

The parameters to be estimated were Y_{HAO}, k_{mO2} and the ratio V_{maxeTO}/V_{maxeD} using equation 10. Parameters were estimated by minimising the squared difference between model predictions and measurements: electron flow was used as a unit, allowing the N_2O emission from HAO to be converted to electron flow as for denitrification. Thus, the empirically determined electron flow was $V_{eEMP} = V_{N2O} * 2 + V_{NO}$. The model output to be fitted is $V_{eMOD} = V_{eD} + V_{NO2} * Y_{HAO} * 2$, where the factor 2 (mol electrons per mol N_2O-N) is included to allow the N_2O production to emulate an electron flow, in order have a common unit for V_{eMOD} and V_{eEMP}.

The parameters were estimated by "least square", using the problem solver in excel. The general linear regression routine generated the following estimates: Y_{HAO} = 0.0019 (i.e. the constant fraction of oxidized N emitted as N_2O), k_{mO2} = 11.2 µM (i.e. the half saturation constant for terminal oxidases), V_{maxeTO}/V_{maxeD} = 640 (i.e. the ratio between maximum rate of electron flow to terminal oxidases, and the maximum electron flow to denitrification). The model performance far from perfect, as demonstrated in Fig. 6 (main text) and Fig S6. The correlation between model prediction and measured V_{eD} (r^2 = 0.51; Fig S6). It should be noted that Y_{HAO} is not needed to obtain a reasonable fit: by forcing Y_{HAO} = 0, and estimating only $k_{m,O2}$ and V_{maxeTO}/V_{maxeD}, the correlation between model and measurement is the same, with the new parameter set estimated: k_{mO2} = 4.9 µM O_2, V_{maxeTO}/V_{maxeD} = 279. The implication is that it is not necessary to assume that a constant fraction of the oxidized N is emitted as N_2O by incomplete hydroxylamine oxidation to "explain" the observations.

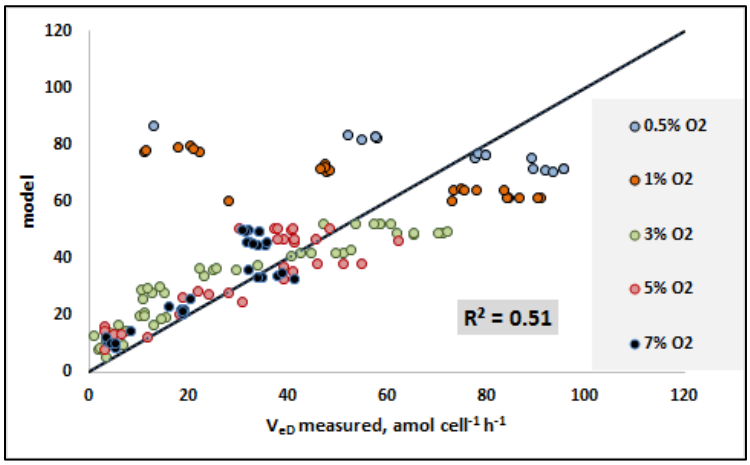

Fig. S6. Model versus measurement of V_{eD}. The modelled V_{eD} (amol $cell^{-1}$ h^{-1}) includes N_2O from incomplete hydroxylamine oxidation (assuming 2 mol e^- mol^{-1} N_2O-N), to allow comparison with measurements. Model parameters are Y_{HAO} = 0.0019, k_{mO2} = 11.2 µM, V_{maxeTO}/V_{maxeD} = 640. The black line showsn the 1:1 relationship between model and measurements.

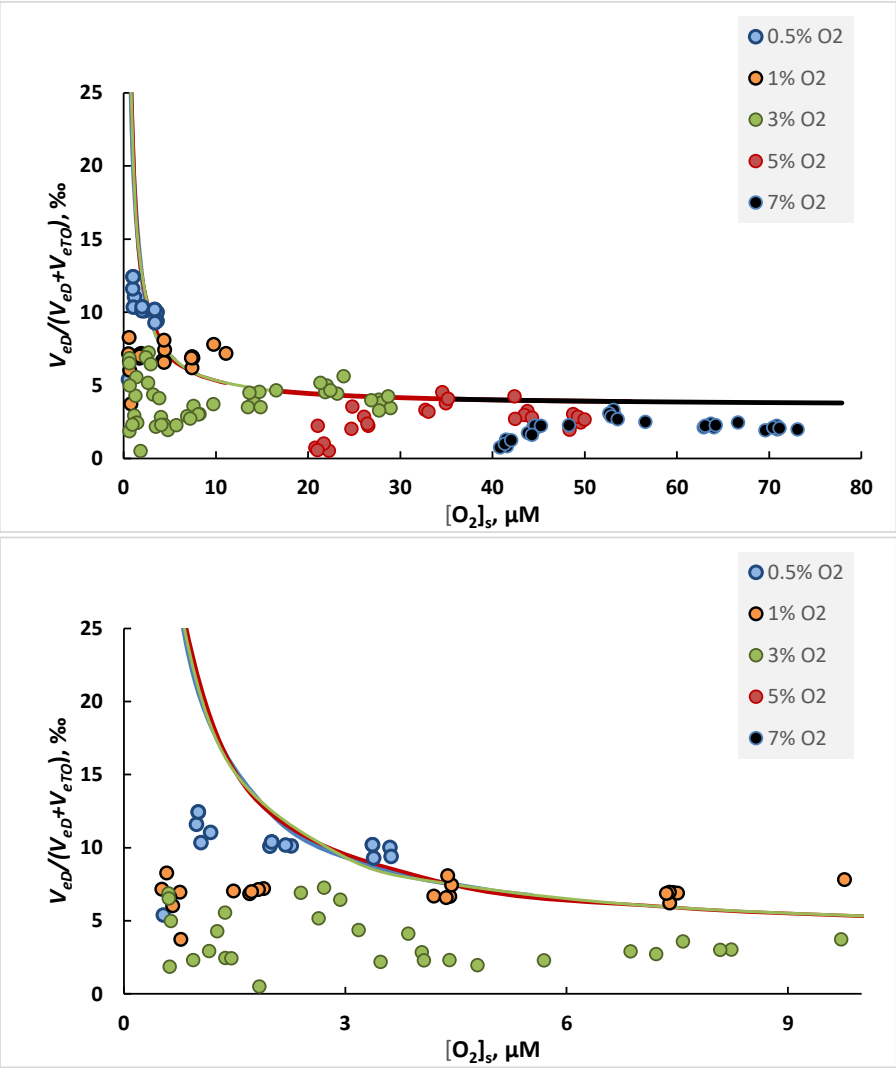

Fig S7. Measured and modelled electron flow to denitrification as a fraction of total ($V_{eD}/(V_{eD}+V_{eTO})$). The panel shows the measured and modelled electron flow to denitrification (V_{eD}, assuming that all N_2O is produced by denitrification, see text and legend Fig S6), expressed as ‰ of the sum of the electron flow denitrification (V_{eD}) and to terminal oxidases (V_{eTO}), plotted against the oxygen concentration at the cell surface ($[O_2]_s$). Upper panel shows the entire dataset, lower panel shows the data for 0-10 µM O_2.

Parameterisation, assuming different affinities for C_{552}

The simplified model, based on the assumption that terminal oxidases and denitrification enzymes have identical affinity for C_{552} gave reasonable fit for high O_2 concentration, but clearly not for the very low O_2 concentration range (0 - 5 µM), as seen in Fig. S6 and in the insert of Fig. 6 (main text). While the measured electron flow declined gradually with $[O_2]$ within the range 0 - 3 µM, the model predicted an increased electron flow to denitrification until $[O_2]$ reached < 0.2 µM.

This was explored with a model exercise with the more complicated approach, using dynamic simulation of $[C^*_{552}]$ to find the steady state concentration for each set of conditions (i.e. $[O_2]$ and $[NH_4^+]$). This allowed exploration of the effect of different affinities to C_{552} (TO versus D). To simplify the modelling exercise, model outputs (i.e. V_{eD}) were compared with measurements for the 1 mM TAN experiments, limited to the time increments when [TAN] was >0.7 mM. An average TAN concentration of 0.8 mM was assumed for these simulations. V_{eR} was estimated as in the previous modelling exercise and used to simulate the steady state $[C^*_{552}]$ and V_{eTO} and V_{eD}. The simulations were done with time steps of 1 - 5 x 10^{-3} s and steady state concentrations were reached. The simulations were done for a range of O_2 concentrations and the steady state electron flows were compared by eye with the empirically determined V_{eD}. To avoid the problems of determination of $[C^*_{552}]$ on a volume basis, the unit for $[C^*_{552}]$ and k_{mTO} and k_{mD} were expressed as number of molecule per cell. Predicted numbers of C^*_{552} molecules per cell at steady state ranged from 500 - 5000 for the k_{mTO} and k_{mD} values explored and k_{cat} = 100 - 1000 s^{-1}. The model output in terms of V_{eD} was unaffected by proportional changes in k_{mTO} and k_{mD} (i.e. increasing or decreasing both with the same factor), but it affected the steady state C^*_{552}.

The result of two simulations are shown in Fig. S8. The red line is the model fitted to the entire dataset. In an attempt to fit the model to data for the low O_2 concentration range, increased affinity of the terminal oxidases for O_2 (reduction of k_{mO2} to 0.4 µM) was simulated, resulting in increasing V_{eD} with increasing $[O_2]$ (as measured), but the level was much too low (blue line). A reasonable fit between model and measurement for the lower O_2 concentration range was achieved by additionally increasing V_{maxeD} by a factor of 4 (black line). However, this parameter set resulted in much too high V_{eD} values for the high O_2 concentration range.

This failure of the model provides a hypothesis-generating observation. In trying to fit the model to the results for the low O_2 concentration range, two changes were made: lowering k_{mO2} and increasing V_{maxeD}. Both are in fact plausible regulatory responses to O_2 limitation: expression of high affinity terminal oxidases (lowering the effective k_{mO2}) and expressing more denitrification enzymes (increasing V_{maxeD}). Thus, the model failure could be taken to suggest a plausible regulatory response to O_2 limitation.

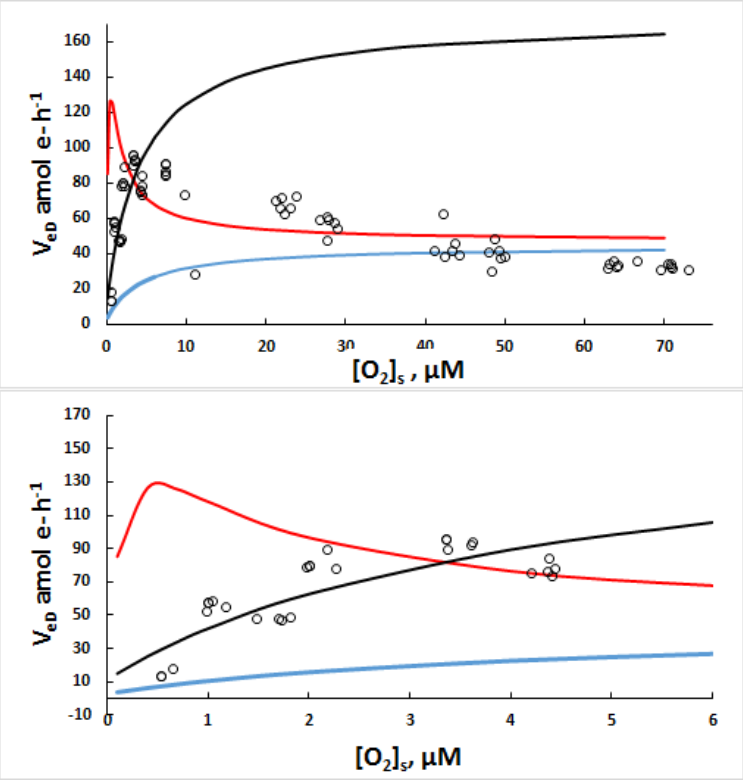

Fig. S8. Attempts to simulate V_{eD}, assuming that TO and D have different affinities for C_{552}. The panels show model predictions measurement based estimated of electron flow to denitrification in the 1 mM TAN experiment with *N. europaea*, limited to the time increments when TAN>0.7 mM. The red line is the prediction assuming $k_{mD} = 70*k_{mTO}$ (k_{mTO} = 600 molecules per cell), k_{mO2} = 4 µM, V_{maxeD} = 3 fmol e^- $cell^{-1}$ h^{-1}, V_{maxeTO} = 20 fmol e^- $cell^{-1}$ h^{-1}. As for the simpler model (Fig. 3, main text), this simulation failed to capture the gradual decline in V_{eD} with declining $[O_2]$ within the concentration range 0 - 4 µM. By lowering k_{mO2} to 0.4 µM, the model predicted such a response, but the level was much too low (blue line). But combining this low k_{mO2} with increased V_{maxeD}, the model is in touch with the observations for the 0 - 4 mM O_2 range (black solid line). However, this parameter set grossly overestimated V_{eD} for the high O_2 concentration range (black dashed line). The shift in parameter values from the red line to the black line could be a plausible regulatory response to O_2 limitation: expression of high affinity terminal oxidases and increased expression of denitrification enzymes.

3. Modelling electron flow in *Nitrosomonas europaea* grown at 4 mM TAN

Attempts to use the parameterised model (based on the 1 mM TAN experiment with *N. europaea*) to predict the high N_2O production at 4 mM compared to that at 1 mM were of no value, since the cell-specific O_2 consumption, growth rate and yield were lower at 4 than at 1 mM TAN. However, in parameterising the model the 4 mM TAN experimental data were of interest. A meaningful use of the model requires determination of the parameters for cell-specific O_2 consumption rate; equation 9 (equation 4, main text). Since none of the treatments depleted TAN (in the vials with 7% O_2, the TAN concentration was ~1.5 mM when O_2 was depleted), determination of the affinity for TAN was impossible, but the affinity for O_2 and the apparent maximum rate of O_2 consumption (V_{max}, equation 9) could be determined (Fig. S9).

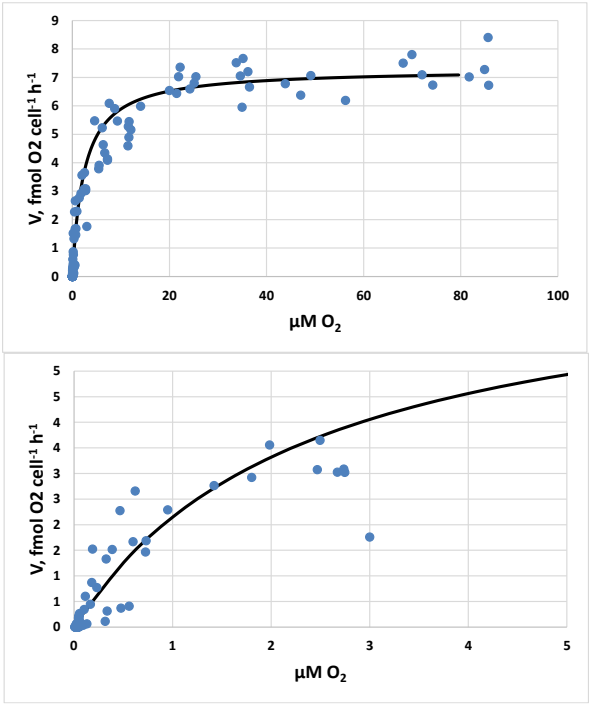

Fig. S9. Oxygen-dependent cell-specific O_2 consumption kinetics of *Nitrosomonas europaea* with 4 mM TAN. A Michaelis-Menten function ($V = V_{max} * [O_2]_* ([O_2] + k_{mO2})^{-1}$ was fitted to the measured values, with the k_{mO2} value obtained for the 1 mM TAN experiment (2.4 µM), but with a much lower V_{max} (7.3 fmol O_2 cell^{-1} h^{-1}). The top panel shows the entire O_2 concentration range; the bottom panel only low O_2 concentrations 0 - 5 µM O_2. The exercise suggests that the high TAN concentration slows down the metabolism of *N. europaea*, but the affinity for O_2 is essentially the same as for the 1 mM TAN experiment.

Using these values, and the k_{mTAN}= 0.565 mM, attempts were made to fit a simpler model (assuming $k_{mTO} = k_{mO2}$) to data. Although a parameter set was found, the model is not statistically significant (r^2 = 0.003), reflecting the gross variation in this dataset, as illustrated in Fig. S10. The figure includes a model curve (red line) for predicted V_{eD} when using the model parameters

determined for the 1 mM TAN experiment. This prediction is 2 - 3 times lower than the fitted model and only approaches empirical data at very low O_2 concentration.

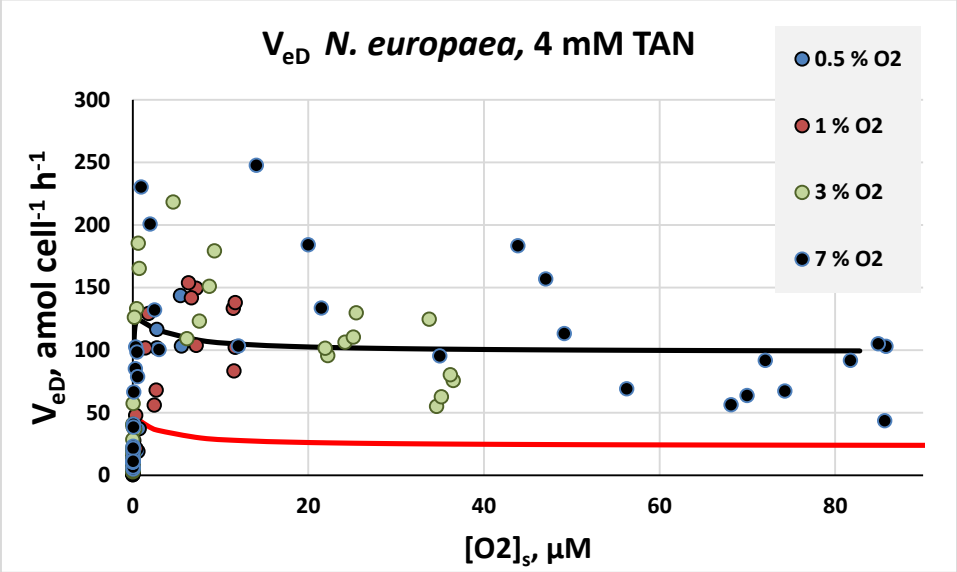

Fig. S10. Assessment of electron flow to denitrification in *Nitrosomonas europaea* when grown with 4 mM TAN. The model when fitted to experimental data resulted in the parameters Y_{HAO} = 6.6‰, $k_{m,O2}$ = 7.5 µM, V_{maxeTO}/V_{maxeD} = 184. The model performance is illustrated by the black line, which is the model prediction for 3 mM TAN. Although the concentration of TAN declined throughout incubation, it remained >>k_{mTAN} even in the vials with 7% O_2 (alternative model predictions with 2 and 4 mM TAN were 92 and 104% of that for TAN = 3 mM). The red line shows model predictions if adopting model parameters from the 1 mM TAN experiment (Y_{HAO} = 0.34‰, k_{mO2} = 5.96 µM, V_{maxeTO}/V_{maxeD} = 410).

References

Whittaker, M., Bergman, D., Arciero, D. and Hooper, A.B. (2000) Electron transfer during the oxidation of ammonia by the chemolithotrophic bacterium *Nitrosomonas europaea*. Biochim. Biophys. Acta 1459:346-355.